Informes Técnicos Ciemat **1049**
Diciembre, 2004

Thermo-Hydro-Mechanical Characterisation of the Bentonite of a Simulated HLW Repository after Five Years Operation (*In Situ* Test of the FEBEX Project)

M.V. Villar

Departamento de Impacto Ambiental de la Energía

Thermo-Hydro-Mechanical Characterisation of the Bentonite of a Simulated HLW Repository after Five Years Operation (*In Situ* Test of the FEBEX Project)

Villar, M.v.

67 pp. 60 figs. 20 refs.

Abstract:

After five years of operation, heater 1 of the FEBEX experiment at the Grimsel Test Site was switched off in February 2002. Following cooling of the system, the bentonite barrier was dismantled and the heater extracted. During dismantling many bentonite samples were taken. Several determinations were carried out in these samples with the aim of: (1) characterise the actual state of the bentonite and (2) determine the possible changes in its properties occurred during the experiment. The results of the thermo-hydro-mechanical characterisation performed at CIEMAT are reported and analysed.
The distribution of water content and dry density of the bentonite in vertical sections presents axial symmetry. The construction gaps of the barrier have been filled by the expansion of the bentonite. The water retention capacity, the hydraulic conductivity and the swelling capacity of the samples from Grimsel have not irreversible changed. The preconsolidation pressure of the Grimsel samples has decreased due to the microstructural changes associated to the volume increase experienced during hydration. The thermal conductivity is higher for the bentonite blocks of the external ring of the barrier.

Caracterizacion Termo-Hidro-Mecánica de la Bentonita de un Almacenamiento Simulado de RRAA tras Cinco Años de Operación (Ensayo *In Situ* del Proyecto FEBEX)

Villar, M.V.

67 pp. 60 figs. 20 refs.

Resumen:

El calentador 1 del ensayo FEBEX realizado en el Grimsel Test Site se apagó en febrero de 2002 tras cinco años de operación. Despues de cuatro meses de enfriamiento del sistema, se desmanteló la barrera de bentonita y se extrajo el calentador. Durante el desmantelamiento se tomaron numerosas muestras de bentonita, en las que se realizaron varias determinaciones con el objeto de: (1) caracterizar el estado de la barrera de bentonita y (2) determinar los cambios en propiedades ocurridos durante la operación. En este informe se describen y analizan los resultados de la caracterización termo-hidro-mecánica realiazada por el CIEMAT.
La distribución de humedad y densidad seca de la bentonita en secciones verticales presenta simetría axial. La expansión de la bentonita al hidratarse ha rellenado los huecos de construcción de la barrera. La capacidad de retención de agua, la conductividad hidráulica y la capacidad de hinchamiento de las muestras de Grimsel no han cambiado irreversiblemente. La presión de preconsolidación de las muestras de Grimsel se ha reducido debido a los cambios microestructurales asociados al aumento de volumen experimentado durante la hidratación. La conductividad térmica es mayor para los bloques de bentonita del anillo externo.

CLASIFICACIÓN DOE Y DESCRIPTORES

S11
HIGH-LEVEL RADIOACTIVE WASTES; THERMODYNAMIC PROPERTIES; MECHANICAL PROPERTIES; CLAYS; GEOCHEMISTRY; RADIOACTIVE WASTE STORAGE; MATHEMATICAL MODELS; COMPUTER CODES; CHEMICAL PROPERTIES; BENTONITE; RADIOACTIVE WASTE STORAGE

Thermo-hydro-mechanical characterisation of the bentonite of a simulated HLW repository after five years operation (*in situ* test of the FEBEX Project)

AUTHOR: M.V. Villar

December 2004

Thermo-hydro-mechanical characterisation of the bentonite of a simulated HLW repository after five years operation (*in situ* test of the FEBEX Project)

Villar, M.V.

61 pp. 60 figs. 20 refs.

Abstract:

After five years of operation, heater 1 of the FEBEX experiment at the Grimsel Test Site was switched off in February 2002. Following cooling of the system, the bentonite barrier was dismantled and the heater extracted. During dismantling many bentonite samples were taken. Several determinations were carried out in these samples with the aim of: (1) characterise the actual state of the bentonite and (2) determine the possible changes in its properties occurred during the experiment. The results of the thermo-hydro-mechanical characterisation performed at CIEMAT are reported and analysed.

The distribution of water content and dry density of the bentonite in vertical sections presents axial symmetry. The construction gaps of the barrier have been filled by the expansion of the bentonite. The water retention capacity, the hydraulic conductivity and the swelling capacity of the samples from Grimsel have not irreversibly changed. The preconsolidation pressure of the Grimsel samples has decreased due to the microstructural changes associated to the volume increase experienced during hydration. The thermal conductivity is higher for the bentonite blocks of the external ring of the barrier.

Caracterización termo-hidro-mecánica de la bentonita de un almacenamiento simulado de RRAA tras cinco años de operación (ensayo *in situ* del Proyecto FEBEX)

Villar, M.V.

61 pp. 60 figs. 20 refs.

Resumen:

El calentador 1 del ensayo FEBEX realizado en el Grimsel Test Site se apagó en febrero de 2002 tras cinco años de operación. Después de cuatro meses de enfriamiento del sistema, se desmanteló la barrera de bentonita y se extrajo el calentador. Durante el desmantelamiento se tomaron numerosas muestras de bentonita, en las que se realizaron varias determinaciones con el objeto de: (1) caracterizar el estado de la barrera de bentonita y (2) determinar los cambios en propiedades ocurridos durante la operación. En este informe se describen y analizan los resultados de la caracterización termo-hidro-mecánica realizada por CIEMAT.

La distribución de humedad y densidad seca de la bentonita en secciones verticales presenta simetría axial. La expansión de la bentonita al hidratarse ha rellenado los huecos de construcción de la barrera. La capacidad de retención de agua, la conductividad hidráulica y la capacidad de hinchamiento de las muestras de Grimsel no han cambiado irreversiblemente. La presión de preconsolidación de las muestras de Grimsel se ha reducido debido a los cambios microestructurales asociados al aumento de volumen experimentado durante la hidratación. La conductividad térmica es mayor para los bloques de bentonita del anillo externo.

Thermo-hydro-mechanical characterisation of the bentonite of a simulated HLW repository after five years operation (*in situ* test of the FEBEX Project)

Table of contents

1. INTRODUCTION

The aim of FEBEX (Full-scale Engineered Barriers Experiment) is to study the behaviour of components in the near-field for a high-level radioactive waste (HLW) repository in crystalline rock. The experimental work consists of three main parts:

- an "in situ" test, under natural conditions and at full scale, performed at the Grimsel Test Site (GTS, Switzerland);

- a "mock-up" test, at almost full scale, performed at CIEMAT facilities (Madrid); and

- a series of laboratory tests to complement the information from the two large-scale tests.

The project is based on the Spanish reference concept for disposal of radioactive waste in crystalline rock (AGP Granito): the waste canisters are placed horizontally in drifts and surrounded by a clay barrier constructed from highly-compacted bentonite blocks (ENRESA 1995). In the two large-scale tests, the thermal effect of the wastes is simulated by means of heaters, whereas hydration is natural in the *in situ* test and controlled in the one performed on the mock-up. Both tests are monitored, this allowing the evolution of the temperature, total pressure, water content, water pressure, displacements and other parameters to be obtained continuously in different parts of the barrier and the host rock, this information being used as a contrast to the predictions of the thermo-hydro-mechanical (THM) and themo-hydro-geochemical (THG) models.

The *in situ* test is performed in a gallery excavated in the underground laboratory managed by NAGRA at Grimsel (Switzerland). The basic components of the test are (Figure 1): the gallery, measuring 70 m in length and 2.3 m in diameter; the heating system, made up of two heaters placed inside a liner installed concentrically with the gallery and separated one from the other by a distance of 1.0 m, with dimensions and weights analogous to those of the real canisters; the clay barrier, formed by blocks of compacted bentonite; the instrumentation and the monitoring and control system for data acquisition and supervision and control of the test both autonomously and remotely, from Madrid. The gallery was excavated through the Aare granite and it crosses a lamprophyre dike in the zone where the first heater was placed (ENRESA 1998a). It is closed by a concrete plug.

To build the clay barrier, various types of blocks were manufactured from the bentonite in the shape of 12-cm thick circular crown sectors. The blocks were arranged in vertical slices giving place to the geometry of the barrier shown in Figure 2 for the heater and non-heater areas. In both areas, the three exterior rings are equal; in the heater area the interior ring is in contact with the steel liner. The blocks were obtained through uniaxial compaction of the FEBEX clay with its hygroscopic water content at pressures of between 40 and 45 MPa, what gave place to dry densities of 1.69-1.70 g/cm^3 and block weights of between 18 and 23 kg. The initial dry density of the blocks was selected by taking into account the probable volume of the construction gaps and the need to have a barrier with an average dry density of 1.60 g/cm^3 (ENRESA 2000).

The heating stage of the *in situ* test, known as operational stage, began on February 27th 1997. After five years of operation, the heater closer to the gallery entrance was switched off (February 2002). After cooling of the system during four months, the bentonite barrier in front of and around the heater was dismantled and the heater extracted (Bárcena *et al.* 2003).

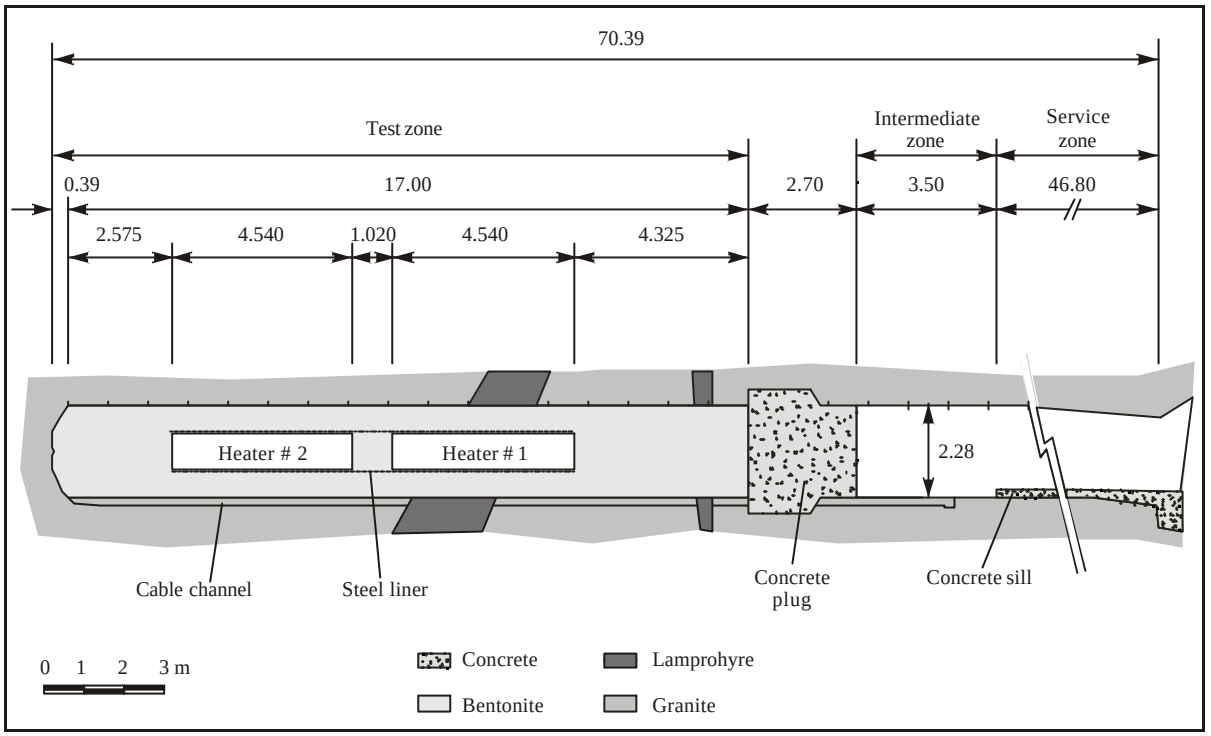

Figure 1: General disposition of principal elements in the test zone before dismantling (ENRESA 2000)

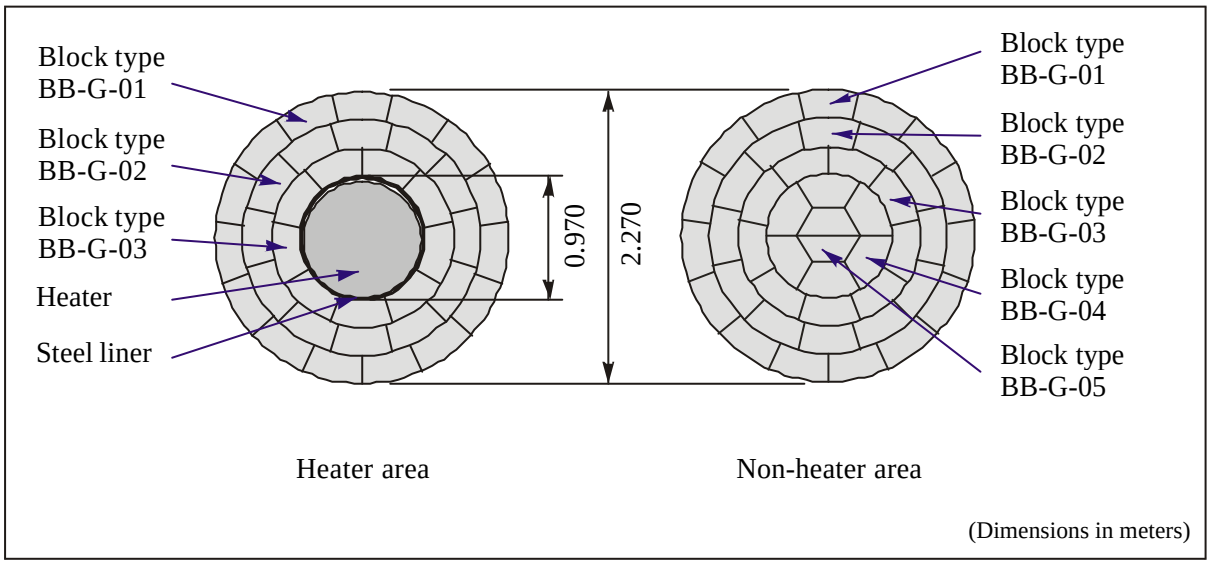

Figure 2: Geometry of the clay barrier in the FEBEX *in situ* test at GTS (ENRESA 2000)

The engineered barriers (waste, canister, and clay barrier) are key elements in the final disposal concept for HLW. The clay barrier has the multiple purpose of providing mechanical stability for the canister, by absorbing stress and deformations, of sealing discontinuities in the adjacent rock and retarding the arrival of groundwater at the canister and of retaining/retarding the migration of the radionuclides released, once failure of the canister and lixiviation of the spent fuel have occurred.

The behaviour of a HLW repository is determined, to a large extent, by the characteristics of the design and construction of the engineered barriers and especially by the changes that may occur in the mechanical, hydraulic, and geochemical properties as a result of the combined effects of heat

generated by the radioactive decay and of the water and solutes contributed by the surrounding rock. Therefore, in FEBEX I and II, it was considered of fundamental importance that the processes taking place in the near-field be understood and quantified, for the evaluation of long-term behaviour. As a consequence, a program of laboratory tests was designed to study and comprehend the processes that take place in the clay barrier under simple and controlled conditions and to develop the governing equations. Additionally, the partial dismantling of the FEBEX *in situ* test carried out at the Grimsel Test Site (GTS) provides the opportunity to check the predictions of the models and the modifications experienced by the bentonite in a direct and representative way.

During dismantling many bentonite samples –in the form of cores or of complete blocks– were taken according to an exhaustive postmortem bentonite sampling and analysis program designed and described in the FEBEX II Test Plan and in the Sampling Book (AITEMIN 2000, Villar *et al.* 2002a). Basically, it consisted on taking samples from different parts of the clay buffer to characterise the solid and liquid phases, in order to confirm predictions and validate existing models of THM and THG processes.

Therefore, the main objectives of the bentonite sampling and analyses program are:

- The characterisation of the state of the barrier, with respect to water contents and densities and to the mineralogy and geochemistry of the bentonite and its pore water.

- The identification of physico-chemical alterations in the clay and possible changes in its thermo-hydro-mechanical properties occurred during the experiment, due to the combined effect of temperature, water content, joints and solutes.

The THM tests performed on the sampled blocks can be divided into inter-related groups: tests to determine basic properties, tests to understand the water flow, tests to determine the changes in the mechanical properties of the clay and tests to determine the changes in the thermal properties of the clay. To evaluate the possible changes occurred, the properties of the untreated FEBEX clay are taken as the reference ones. For that, it is also necessary to know how dry density and water content influence the properties of the clay. The data-base acquired during FEBEX I on the properties of the untreated clay (ENRESA 1998b, 2000; CIEMAT 1999; UPC 1999; Villar 2000, 2001, 2002; Lloret *et al*. 2002) and during FEBEX II (Villar *et al*. 2002b, Lloret *et al*. in press) has served as comparison.

This document collects the results obtained by CIEMAT on the THM bentonite analyses performed in laboratory after dismantling.

2. DISMANTLING OF THE BARRIER AND BENTONITE SAMPLING (TASK 122)

The partial dismantling of the FEBEX *in situ* test was carried out during the summer of 2002, after five years of continuous heating during which the temperature at the heater/bentonite contact was maintained at 100 °C. Heater number 1 was switched off four months before starting the dismantling operations, as the temperature in the area affected by the dismantling should be reduced to a level compatible with manual works (25-30 °C). The dismantling operations included the demolition of the concrete plug and the removal of all the bentonite in front of and surrounding the heater. A large number of samples from all types of materials were taken for analysis. The dismantling was carried our causing a minimum disturbance in the section of the test corresponding to the second heater that was kept in operation at all times and remains in place fully operative. Also the process of data acquisition was maintained during the dismantling. A detailed description of the dismantling and sampling operations is given in Bárcena *et al*. (2003).

Also the process of data acquisition was maintained during the dismantling. This allowed to follow the evolution of temperature and relative humidity (among other parameters) during cooling, and to know exactly which were the conditions of the barrier at the moment of dismantling. Thus, in the instrumented section C (see Figure 1 for location), far away from the heater, the temperatures decreased from values between 21 and 23 °C to values around 18 °C. The tendency of the relative humidity evolution recorded by the sensors placed in this section did not change as a consequence of the switching off, but the relative humidity slightly decreased when the adjacent sections started to be dismantled, probably as a consequence of the higher ventilation (Figure 3). In the sections around the heater, the switching off provoked an overall drop of temperature to values around 25 °C (Figure 4), which implied a modification of the relative humidity registered by the sensors. Hence, the relative humidity near the heater increased from values of 20-24 % before switching off to values of 32-52 % just before dismantling, while in the outermost part of the barrier the relative humidity slightly increased as a consequence of cooling (Figure 5).

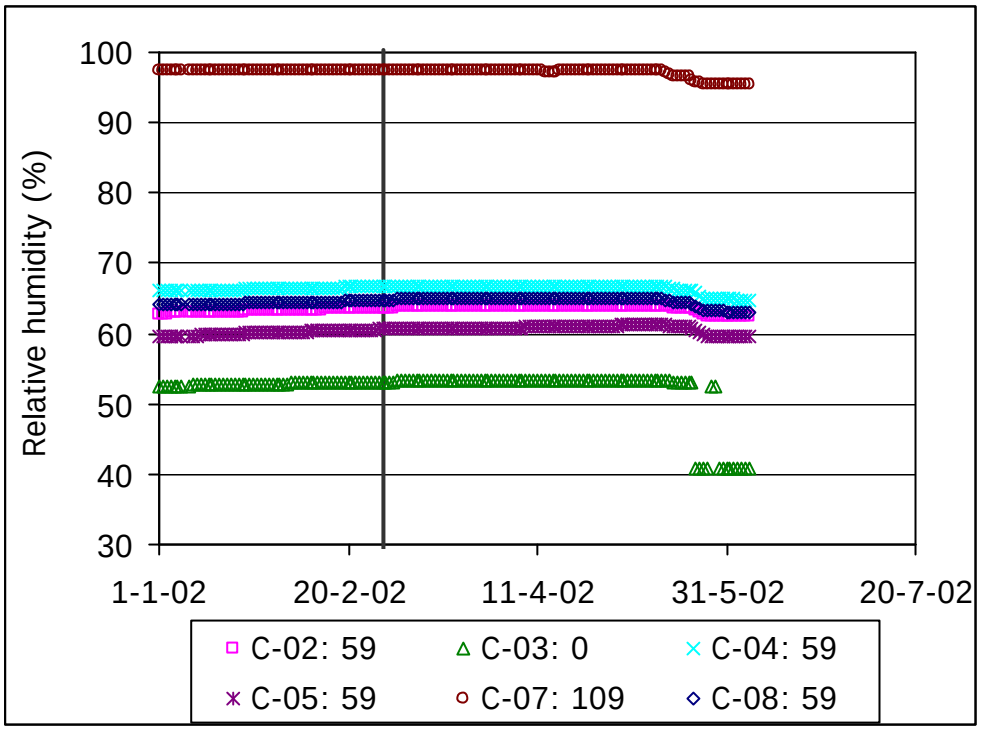

Figure 3: Evolution of the relative humidity registered before dismantling by the capacitive sensors (70-AND-WC) in the instrumented section C (S11). The location of the sensors with respect to the gallery axis is indicated in cm

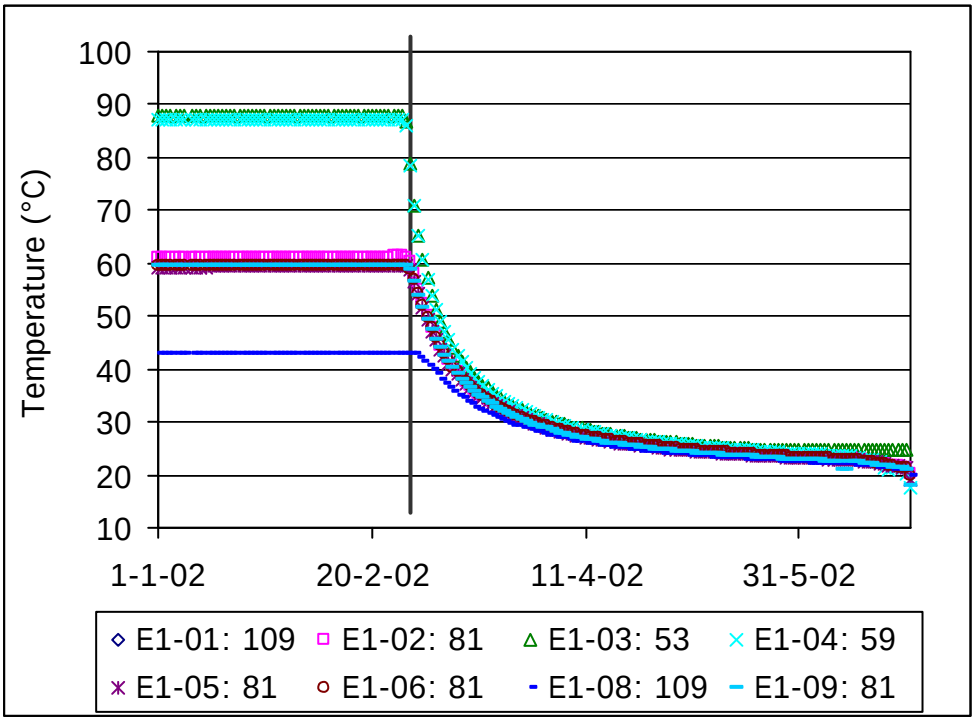

Figure 4: Evolution of the temperature registered before dismantling by the capacitive sensors (70-AND-WC) in the instrumented section E1 (S21). The location of the sensors with respect to the gallery axis is indicated in cm

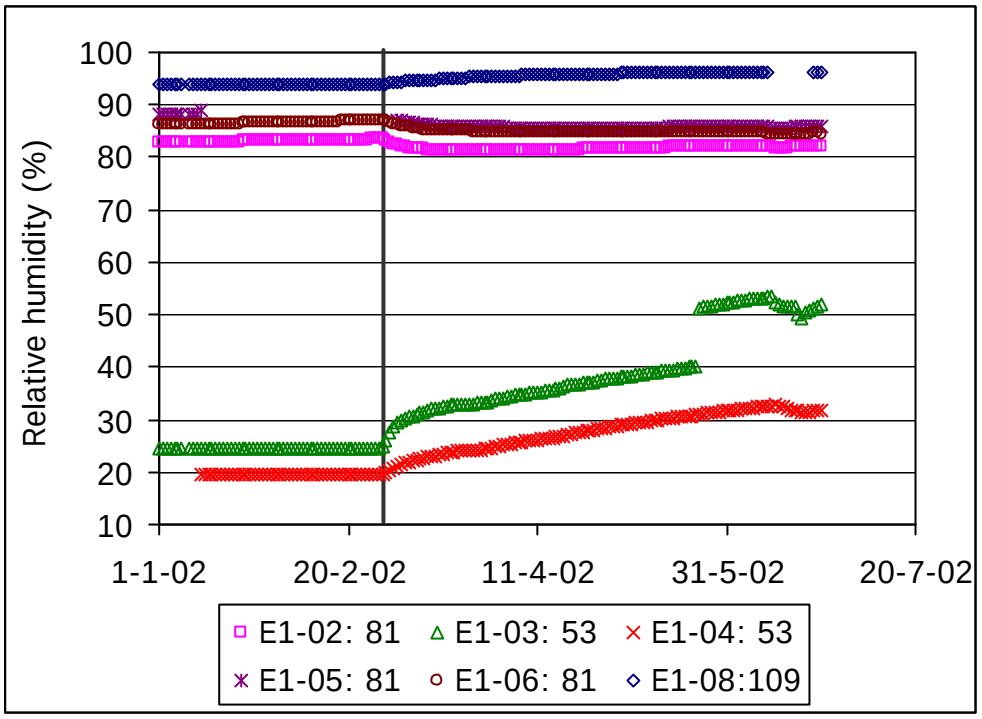

Figure 5: Evolution of the relative humidity registered before dismantling by the capacitive sensors (70-AND-WC) in the instrumented section E1 (S21). The location of the sensors with respect to the gallery axis is indicated in cm

Upon exposure, the bentonite sections presented a consistent appearance; although the joints between blocks were clearly visible, all the construction gaps were sealed, even the big apertures hewn in the bentonite for the passing of the cable bunches (Figure 6). Differences in coloration of the bentonite related to the variations of its water content were observed, the outer rings of the barrier showing darker colours.

Figure 6: Appearance of the bentonite barrier after extraction of the heater

During the dismantling, the radial dimension of some blocks of different slices was measured. The average values obtained in each barrier ring (external, intermediate and internal) of different sections are plotted in Figure 7, along with the initial dimensions of the same kind of blocks. The deviation with respect to the initial dimension has been calculated for each ring and is shown in Table I. It is clear that the higher expansion has taken place in the outer ring, and that the ring closest to the heater has slightly shrunk, due probably to the effect of heating, since this shrinking has not been observed in the sections without heater. In those sections, even the central block (not included in the figure) has swollen.

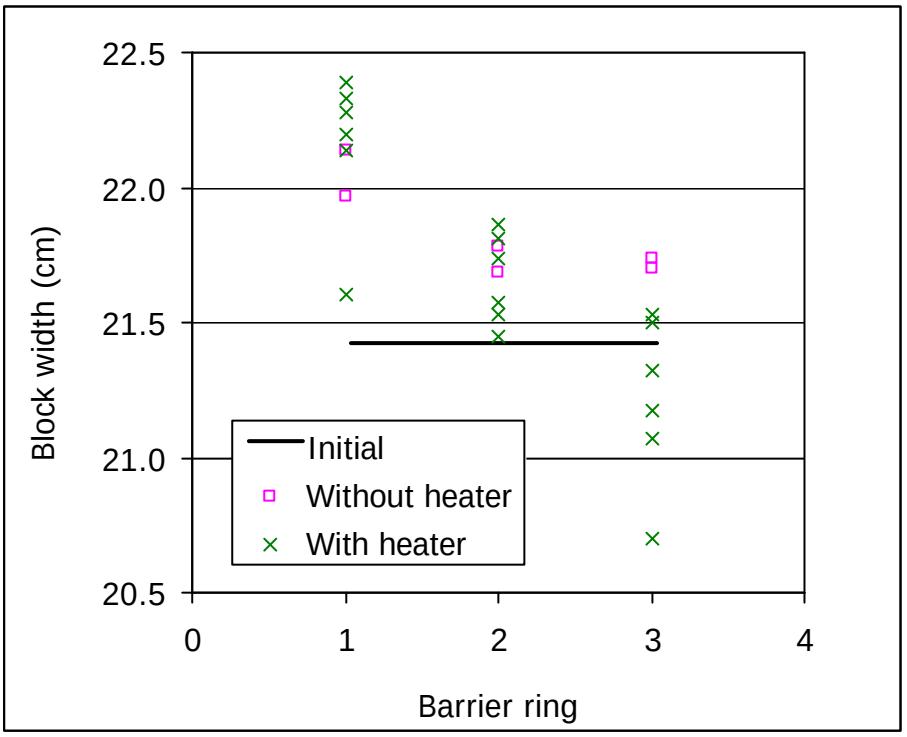

Figure 7: Radial dimension of the blocks in three different rings measured *in situ* during dismantling of several sections (1: external; 2: intermediate; 3: inner)

Table I: Percentage increase of the radial dimension of the blocks

Block type	Sections without heater	Sections with heater
BB-G-01 (external)	3	4
BB-G-02	2	1
BB-G-03	1	-1
BB-G-04 (inner)	6	

The location of the bentonite sampling points was fixed to allow a good representation of physico-chemical alterations and hydration distribution. The sampling took place in vertical sections normal to the axis of the tunnel –corresponding to original block slices–, and in each section several samples were taken along different radii. According to the Sampling Book (AITEMIN 2002), the bentonite samples in which THM characterisation has been performed by CIEMAT were taken from the vertical sections detailed below (Figure 8):

- Four sections in the heater zone: S19, S23, S28 and S31. In sections S23 and S31, 9 intact blocks were taken, following approximately three radii separated 120°, taking the inner, middle and outer block of each radius. From sections S19 and S28, 12 intact blocks were taken, following four radii, taking the inner, middle and outer block of each radius. From these last sections, three blocks belonging to the same radius were transported by CTU to their laboratories in Prague. The rest of the blocks were sent to CIEMAT laboratories.
- In blocks from section S12 –that was sampled in the zone between the concrete seal and the heater for THG characterisation– the thermal conductivity, the dry density and the water content have been determined.
- Several bentonite cores were taken from section S11 (instrumented section C) to determine water content and dry density at the laboratory.
- Blocks from section S25 and S29 –in which tracers were placed– were used for thermal conductivity, dry density and water content determinations.

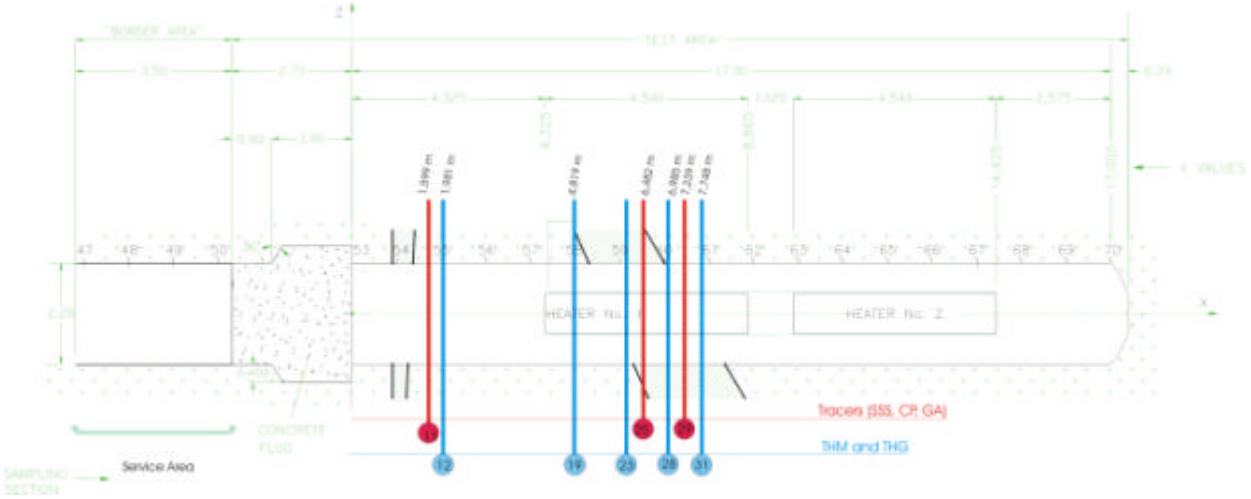

Figure 8: Location of sampling sections used for THM tests by CIEMAT (modified from AITEMIN 2002)

The samples were preserved in plastic film, two layers of aluminised PET-sheets and vacuum-sealed plastic bags immediately after their extraction. The first PET-sheet was vacuum-sealed after flushing nitrogen in it. Protection against mechanical actions was used to ensure the integrity of the material. On the wrapping of every sample, it was clearly indicated its reference and the front and backside with respect to the gallery entrance. The samples were referred to according to the key given in the procedure 070-PC-TA-0002 and the Sampling Book (AITEMIN 2002).

3. BENTONITE ANALYSIS (TASK 141)

The aim of the postmortem THM tests is twofold: (1) to characterise the actual state of the bentonite and (2) to determine the possible changes in its thermo-hydro-mechanical properties occurred during the experiment, due to the combined effect of temperature, water content, joints and solutes. The THM tests can be divided into inter-related groups: tests to determine basic properties, tests for the study of microstructural changes, tests to understand the water flow, tests to determine the changes in the mechanical properties of the clay and tests to determine the changes in the thermal properties of the clay. The database acquired during FEBEX I on the properties of the untreated clay (ENRESA 1998b, 2000; CIEMAT 1999; UPC 1999; Villar 2000, 2001, 2002; Lloret *et al.* 2002) and during FEBEX II (Villar *et al.* 2002, Lloret *et al*. in press) has served as comparison with the reference untreated FEBEX clay.

3.1. SAMPLING AT THE LABORATORY

The laboratory determinations were carried out at CIEMAT facilities from September 2002 to December 2003. Each block was unpacked only once in order to take the subsamples for the different determinations (THG, THM or tracers). The sampling was coordinated so that to be able to make the tests immediately after unpacking and sampling. The blocks have been half-sectioned along the radius, in order to obtain material for the THM and THG tests (Figure 9). The section for THM tests has been referenced with the name of the block followed by the letter A, whereas the section for THG tests has been referenced with the name of the block followed by the letter B. In order to obtain a more detailed sampling, samples have been taken in different positions along the radius of the block. The subsamples obtained in this way have been referenced by adding a correlative number to the initial reference of the block. The numbers have been given starting by the block closer to the gallery wall (Figure 10).

Figure 9: Sectioning of a block for THM (left) and THG determinations (right)

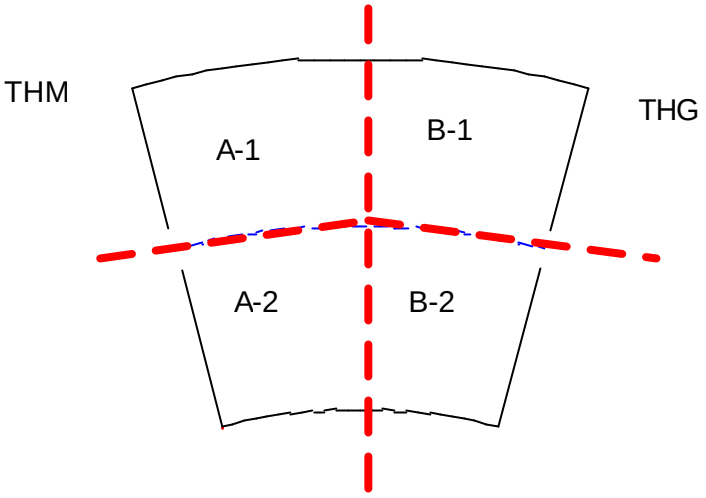

Figure 10: Subsampling of bentonite blocks for THM and THG analyses

All the THM tests have been performed on undisturbed samples that have been obtained mostly by drilling and subsequent trimming to the appropriate dimensions (Figure 9). In those tests in which the sample must be saturated prior to the determination, deionised water has been used.

Figure 11: Drilling of blocks to obtain samples for the THM determinations

3.2. BASIC PROPERTIES: DENSITY AND WATER CONTENT

Blocks bound to THM, THG and tracers determinations have also been sampled for water content and dry density, which have been determined in two different positions of each block along a radius. In the sections without heater, just the three external rings of the sections have been sampled. Consequently, at least six determinations have been made along a given radius of the barrier, whose length is about 114 cm in the sections without heater and 65 cm in the sections with heater. The gravimetric water content (w) has been determined by oven drying at 110 °C during 24 hours, and is defined as the ratio between the weight of water and the weight of dry solid expressed as a percentage. Dry density (ρ_d) is defined as the ratio between the weight of the dry sample and the volume occupied by it prior to drying. The volume of the specimens has been determined by immersing them in a recipient containing mercury and by weighing the mercury displaced, as established in UNE Standard 7045 "Determination of soil porosity."

The results obtained for the different sections sampled are plotted in Figure 12. No differences in water content are noticed between the sections with heater and the sections without heater. The water content increases from the block closer to the heater to the external block in an approximately exponential way. The higher values are around 30 percent and the lower around 15 percent, being the mean value 22 percent. The water contents higher than 30 percent found in some external blocks of section 29 are justified by their proximity to the cable bunch, which is a preferential water pathway. The results obtained in the laboratory have been compared with those obtained *in situ* by CIMNE for nearby sections (Daucausse & Lloret 2003, Figure 13). The agreement between both measurements is very good (except maybe for a tendency to find higher water contents near the gallery wall in the determinations carried out *in situ*), what suggests that the packing and transport conditions have been the appropriate to keep the *in situ* conditions of the blocks even several months after their retrieval.

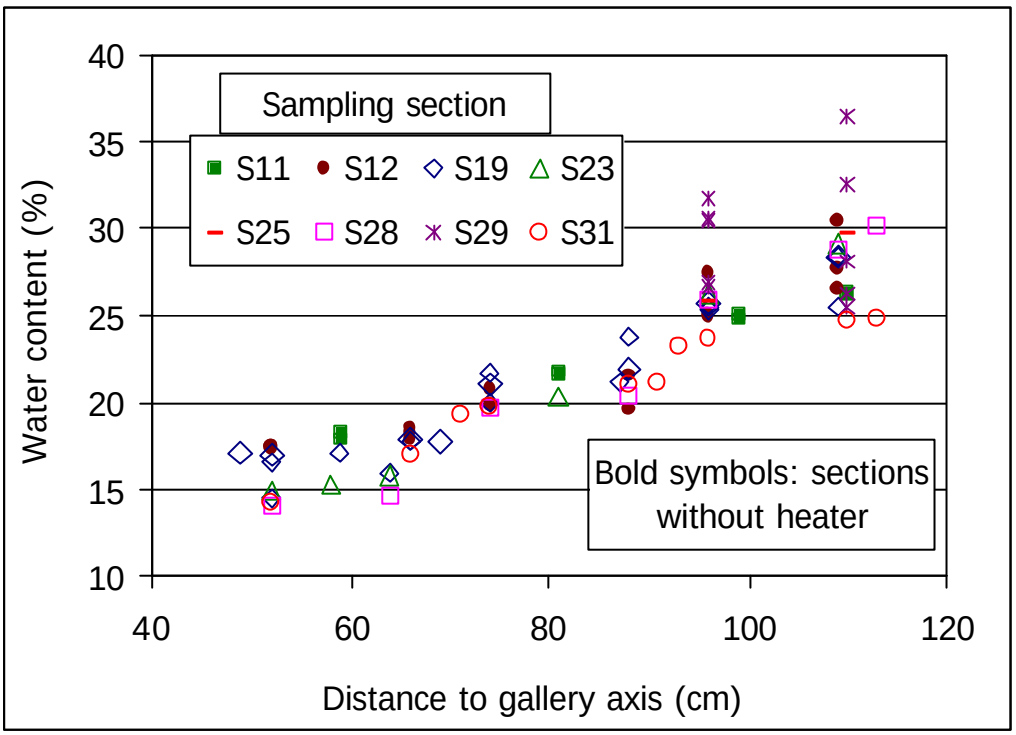

Figure 12: Water contents measured along radius of different sections

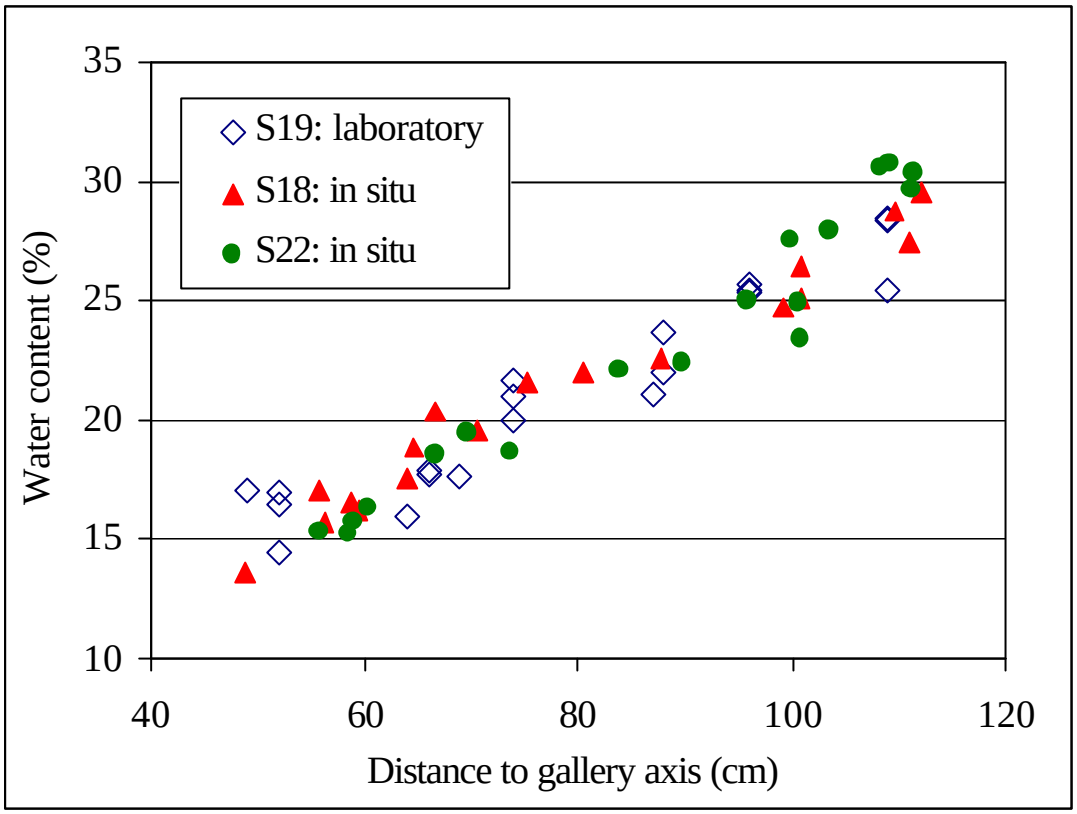

Figure 13: Comparison of water contents measured *in situ* (CIMNE) and in laboratory (CIEMAT)

The dry densities measured are plotted in Figure 14 as a function of the distance to the gallery axis. The arithmetic mean of all the values measured is 1.58 g/cm^3, well bellow the initial dry density of the blocks (which was 1.70 g/cm^3), due to the filling of the construction gaps as a result the expansion caused by saturation. The initial dry density of the blocks was selected by taking into account the probable volume of the construction gaps and the need to have a barrier with an average dry density of 1.60 g/cm^3 (ENRESA 2000). The dry density decrease with respect to the initial one is higher from the heater towards the gallery wall, especially in the blocks closer to the granite. In these blocks, the dry density decreases even below the average dry density of the barrier to values around 1.50 g/cm^3. On the contrary, near the heater the dry density remains around 1.70 g/cm^3, due to the shrinkage caused by the initial desiccation and the compression exerted by the adjacent expanding blocks. These observations agree well with the increase in the radial dimension measured in the blocks of the external ring (Figure 7). Again, the exceptionally low values of dry density (around 1.40 g/cm^3) found in some external samples of section 29 are related to their proximity to the cable bunch.

The results obtained in the laboratory for section S19 have been compared with those obtained *in situ* by CIMNE for the nearby section S18 (Daucausse & Lloret 2003). Despite the fact that the technique employed to determine dry density is different (mercury immersion for CIEMAT, coating with paraffin and weighing the sample first in air and then again while immersed in distilled water for CIMNE), the results obtained agree quite well (Figure 15).

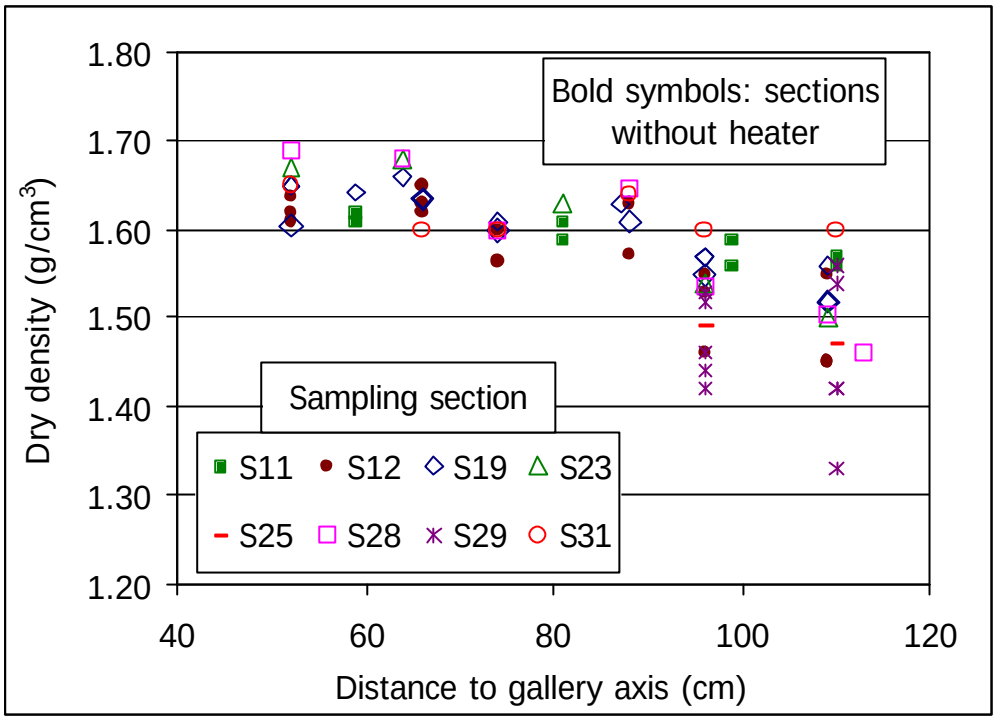

Figure 14: Dry densities measured along radius of different sections

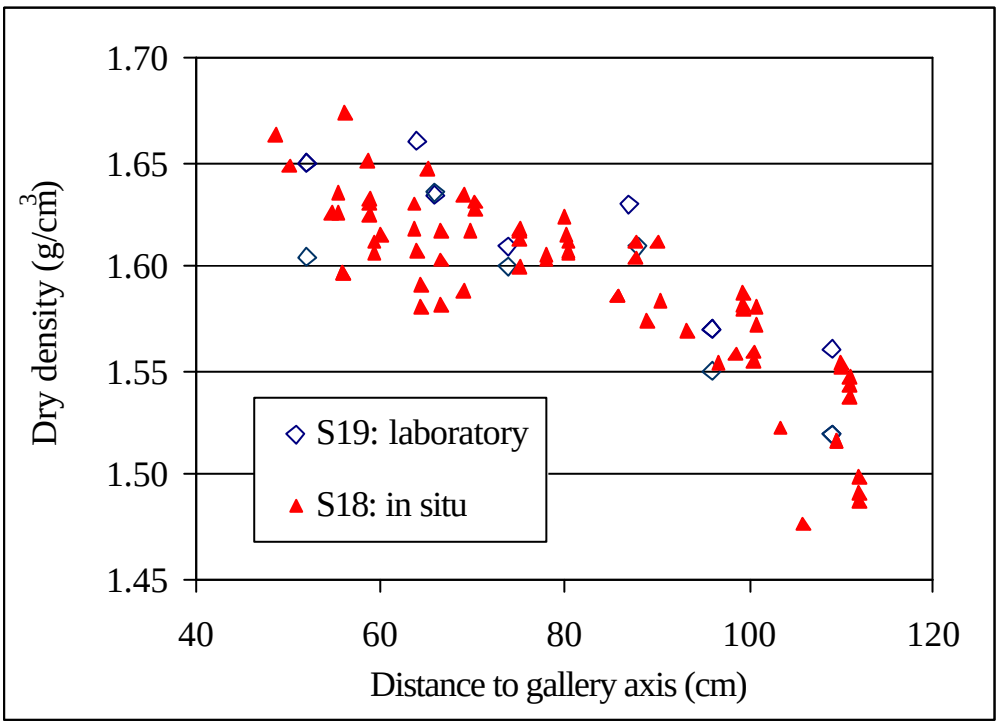

Figure 15: Comparison of dry densities measured *in situ* (CIMNE) and in laboratory (CIEMAT) in two adjacent sections

The degrees of saturation have been calculated for each sample taken into account its dry density and water content and considering a density of water of 1.00 g/cm^3. The values obtained are plotted in Figure 16. There is a clear diminution of the degree of saturation from the gallery wall to the heater surface. The highest values are close to 100 percent, although full saturation is not even reached in the proximity of the gallery wall. This is probably due to the decrease of dry density that

goes with hydration (Figure 14) and to the demand of water by the inner parts of the barrier. The degrees of saturation are higher than 60 percent all through the barrier, and have a mean value of 83 percent.

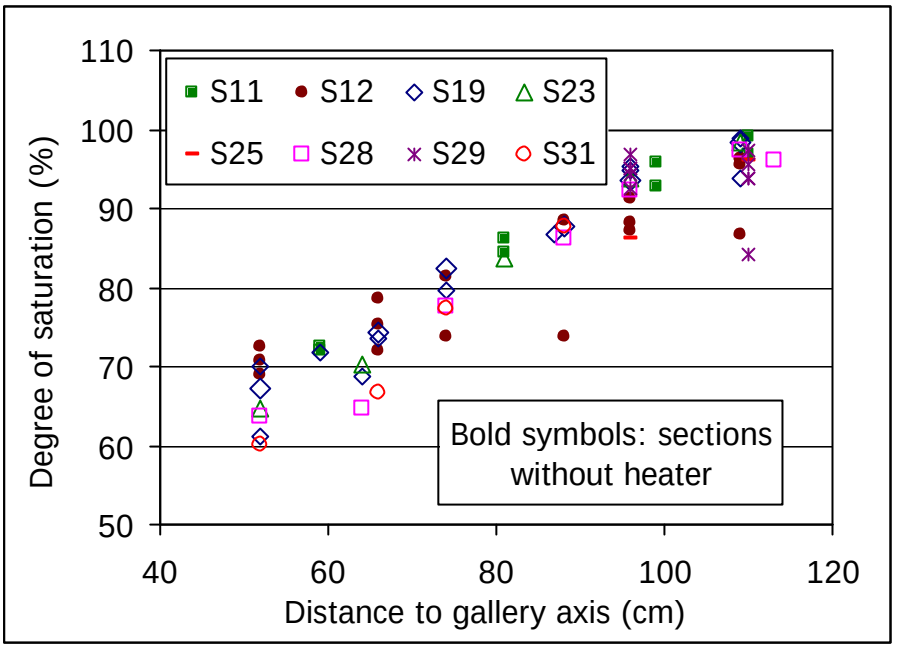

Figure 16: Degree of saturation along radius of different sections

Table II summarises the results presented above as a function of the position of the blocks with respect to the gallery axis.

Table II: Mean values along the barrier of physical characteristics

Position	Dry density (g/cm^3)	Water content (%)	Degree of saturation (%)
External ring of sections without heater	1.53	26.5	93
Medium ring of sections without heater	1.59	20.8	81
Internal ring of sections without heater	1.62	17.9	73
External ring of sections with heater	1.51	27.6	95
Medium ring of sections with heater	1.59	21.8	85
Internal ring of sections with heater	1.65	16.1	67
Average	1.58	22.2	83

These parameters have been also determined in samples from section S7, the one in contact with the concrete plug (Fernández & Rivas 2004). The distribution of dry density and water content throughout the section follows a quite different pattern than in the rest of the sections. For this reason the results are presented separately (Figure 17). The average water content measured is 28.2 percent, and the average dry density 1.48 g/cm^3, much higher and lower, respectively, than the values measured in the rest of the sections (Table II). The fact that the concrete were pumped with a

high water content (ENRESA 2000, p. 209) would cause a sudden increase of the water content of the clay and its swelling. Afterwards, the concrete plug surface may have behaved as a preferential water passageway during the operational phase of the experiment.

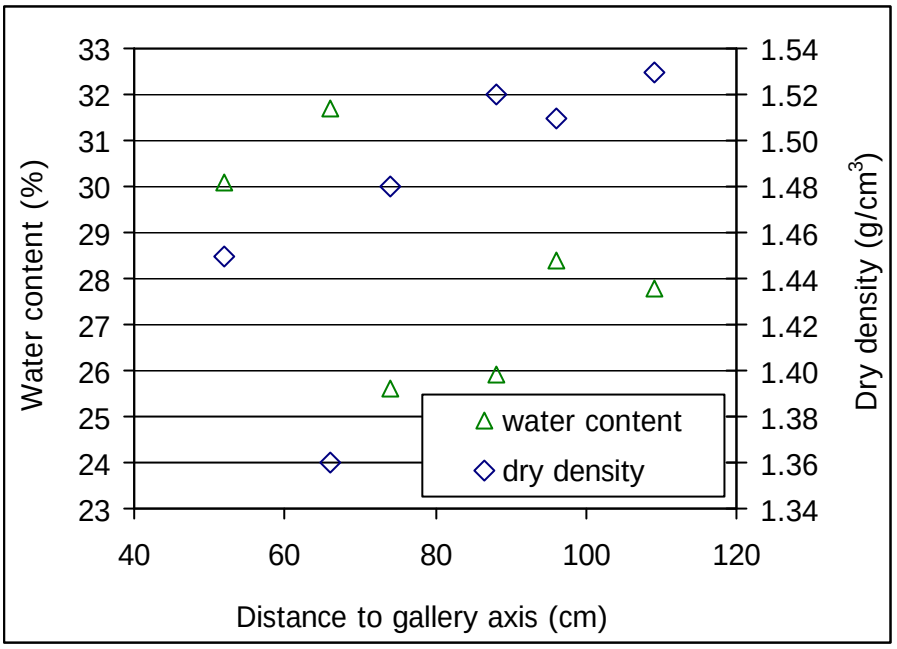

Figure 17: Water contents and dry densities measured along a radius of section S7

3.3. TESTS FOR THE STUDY OF MICROSTRUCTURAL CHANGES

3.3.1. Retention curves

The retention curve has been determined for six samples from one of the sampled radii in two sections around the heater (S23 and S31), at the inner, outer and middle ring of the bentonite barrier. Consequently, the samples have been taken from blocks BB23-1, BB23-2, BB23-3, BB31-1, BB31-2, BB31-3. Two samples of each block have been trimmed with cylindrical cutters. The resulting height of the specimens was between 1.3 and 1.6 cm and their diameter was of 3.4 cm for samples from section S23 and between 3.3 and 5.1 cm for samples from section S31.

The specimens thus prepared were placed in desiccators with sulphuric acid (Figure 18), so that to apply a given suction to the samples by means of the control of the relative humidity. The samples are not confined during the determination and they can freely swell or shrink. The samples were initially submitted to a suction of 4 MPa, what meant for most of them an increase of water content and a decrease of dry density. Afterwards they were progressively dried by applying increasingly higher suctions: 14, 33, 75 and 120 MPa. The latter value corresponds approximately to the suction the blocks had prior to their installation in Grimsel (room temperature and relative humidity.) The samples were subjected to each suction for at least two months, a period of time to guarantee equilibrium. After each suction step the samples were weighed and measured to determine their water content and dry density. Likewise, the final density of the sulphuric acid solution in the desiccator is checked, using a pycnometer. This gives the exact value of suction to which the samples were subjected. Once the retention curve determination completed, the samples were measured and dried in the oven at 110 °C for 24 hours to check their final density and water content. The determinations were performed at 20 °C.

Figure 18: Desiccator with the trimmed samples inside

The results obtained for section S23 are presented in Table III and for section S31 in Table IV. The water content, dry density and degree of saturation of each sample at the beginning of the tests and after equilibrium with each suction are shown. The samples closer to the gallery wall had initial higher water contents and lower dry densities. After being subjected to a suction of 4 MPa most of the samples experienced a density decrease and an increase of water content, except for the samples taken from the block closer to the gallery wall in section S23 (BB23-1-1 and BB23-1-2) whose water contents barely changed. In the following suction steps the water content of all the samples progressively decreased and the dry density increased. The evolution of all the samples is quite similar, despite their positions in the barrier. This can be clearly seen in Figure 19 and Figure 20, in which it becomes also patent that the initial differences attenuate as the suction applied is higher. However, the initial differences in dry density among the different samples remain during the determination of the whole retention curve (Figure 21 and Figure 22): the samples with higher initial dry density swell more during the initial wetting and their density remains lower in the course of the entire determination.

Table III: Retention curves of samples from section S23

Position[1]	Suction:	Initial	4 MPa	14 MPa	33 MPa	75 MPa	120 MPa
BB23-1-1 109 cm	w (%)	26.6	26.8	23.0	19.7	15.4	12.5
	ρ_d (g/cm^3)	1.48	1.47	1.54	1.64	1.70	1.73
	S_r (%)	88	86	83	82	71	60
BB23-1-2 109 cm	w (%)	26.3	26.3	22.2	19.1	15.5	12.5
	ρ_d (g/cm^3)	1.49	1.51	1.60	1.68	1.69	1.78
	S_r (%)	87	91	87	85	70	65
BB23-2-1 80 cm	w (%)	18.6	26.2	21.8	19.0	15.2	12.5
	ρ_d (g/cm^3)	1.60	1.35	1.48	1.54	1.64	1.69
	S_r (%)	73	71	71	68	63	57

Position[1]	Suction:	Initial	4 MPa	14 MPa	33 MPa	75 MPa	120 MPa
BB23-2-2 80 cm	w (%)	18.8	26.3	21.9	19.0	15.2	12.5
	ρ_d (g/cm^3)	1.59	1.33	1.47	1.51	1.61	1.67
	S_r (%)	72	69	70	65	61	55
BB23-3-1 64 cm	w (%)	13.7	26.9	21.9	18.8	14.8	12.2
	ρ_d (g/cm^3)	1.58	1.28	1.35	1.41	1.48	1.55
	S_r (%)	52	65	59	56	49	44
BB23-3-2 52 cm	w (%)	14.1	26.8	22.0	18.8	14.9	12.2
	ρ_d (g/cm^3)	1.57	1.28	1.36	1.46	1.52	1.62
	S_r (%)	53	65	60	59	52	49

[1]Distance to gallery axis

Table IV: Retention curves of samples from section S31

Position[1]	Suction:	Initial	4 MPa	14 MPa	28 MPa	60 MPa	119 MPa
BB31-1-1 109 cm	w (%)	23.8	28.8	24.4	21.6	18.6	14.5
	ρ_d (g/cm^3)	1.54	1.44	1.54	1.60	1.67	1.74
	S_r (%)	85	88	88	85	81	71
BB31-1-2 96 cm	w (%)	22.5	28.1	23.9	21.3	18.5	14.6
	ρ_d (g/cm^3)	1.55	1.45	1.52	1.58	1.62	1.70
	S_r (%)	82	88	83	81	75	67
BB31-2-1 86 cm	w (%)	19.6	28.1	24.1	21.4	18.7	14.8
	ρ_d (g/cm^3)	1.59	1.38	1.45	1.56	1.57	1.66
	S_r (%)	75	80	76	80	70	64
BB31-2-2 74 cm	w (%)	18.6	28.3	24.1	21.0	18.3	14.5
	ρ_d (g/cm^3)	1.51	1.28	1.36	1.46	1.48	1.48
	S_r (%)	64	69	66	67	60	48
BB31-3-1 64 cm	w (%)	15.5	28.2	24.4	21.6	18.8	15.1
	ρ_d (g/cm^3)	1.62	1.31	1.38	1.43	1.48	1.57
	S_r (%)	63	72	68	66	62	56
BB31-3-2 52 cm	w (%)	14.3	26.5	22.8	19.9	17.1	13.1
	ρ_d (g/cm^3)	1.62	1.29	1.36	1.41	1.46	1.52
	S_r (%)	58	66	62	59	55	46

[1]Distance to gallery axis

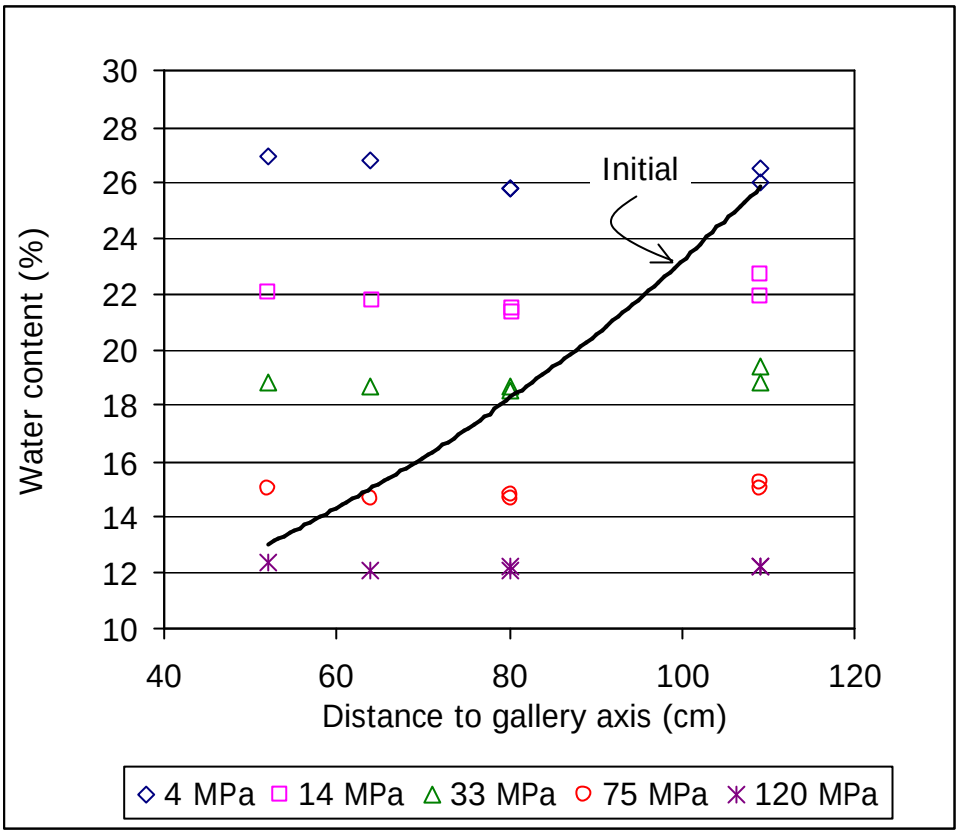

Figure 19: Water contents reached under different suctions for samples from section S23

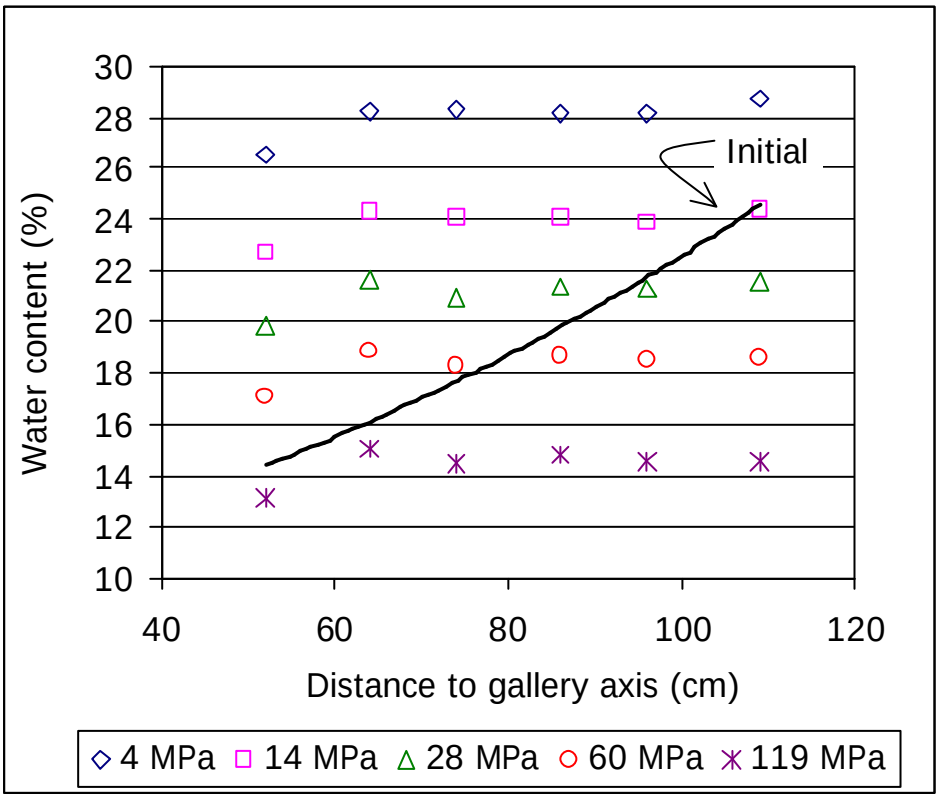

Figure 20: Water contents reached under different suctions for samples from section S31

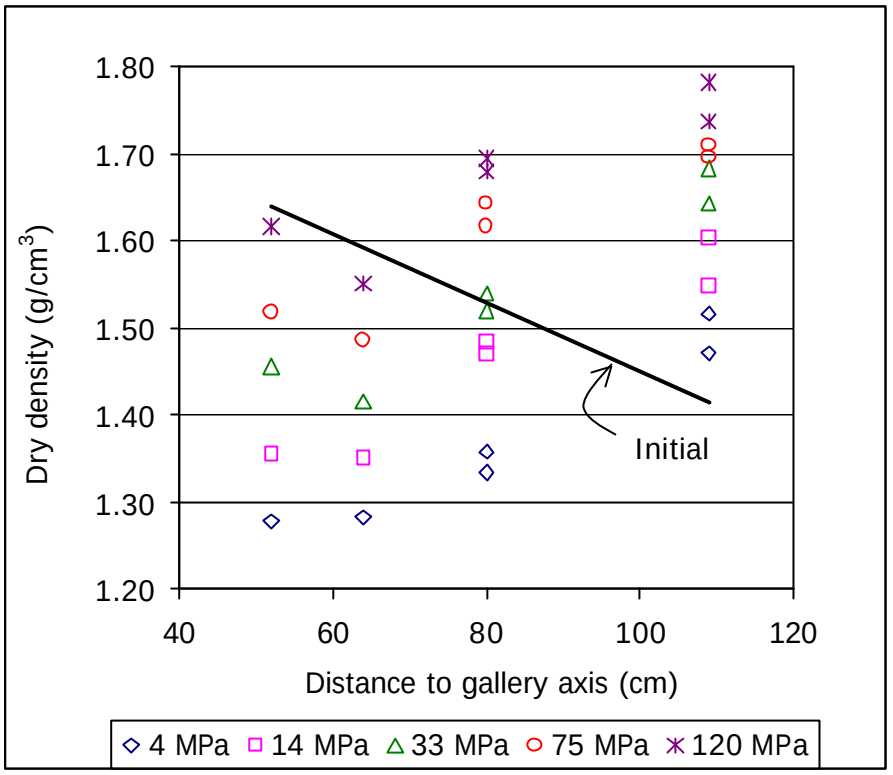

Figure 21: Dry densities reached under different suctions for samples from section S23

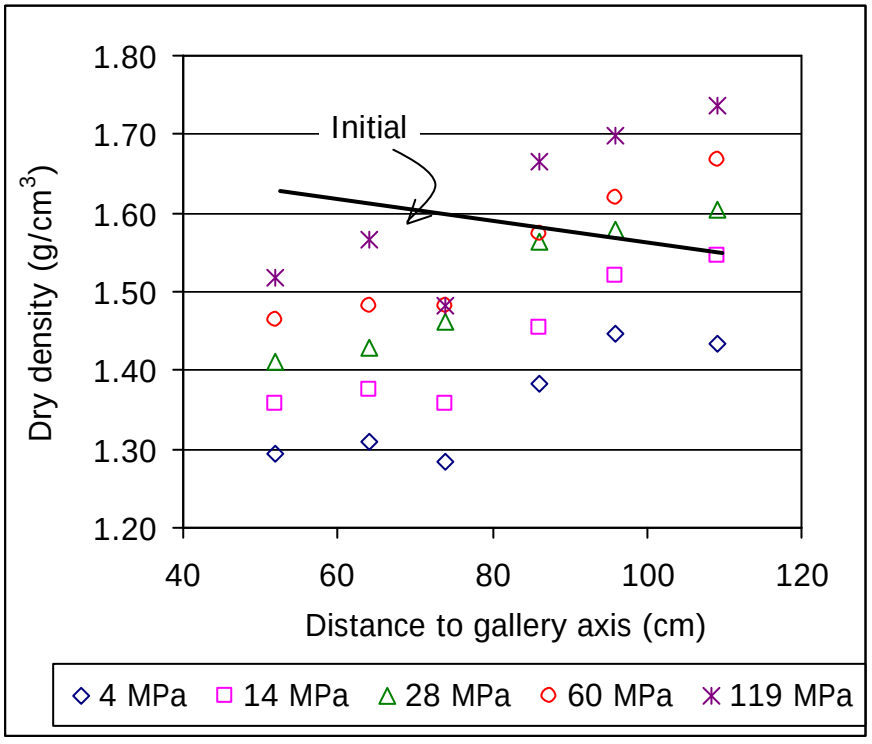

Figure 22: Dry densities reached under different suctions for samples from section S31

In the context of FEBEX I retention curves were determined under free volume conditions for samples compacted at different initial dry densities following various paths (wetting, drying, wetting after drying) (ENRESA 2000, Villar 2002, Lloret *et al*. 2002). Taking into account the results obtained in wetting paths from 148 to 0.1 MPa, an empirical relation between suction (s,

MPa) and water content (w, %) dependent on initial dry density (ρ_{d0}, g/cm^3) has been established, this matching the following expression:

$$w = (-3.79\ \rho_{d0} + 1.42)\ln s + (25.36\ \rho_{d0} - 5.48) \quad [1]$$

The lines obtained with Equation 1 for initial dry densities of 1.40 and 1.60 g/cm^3 have been drawn in Figure 23 together with the results obtained for the samples from section S23. The results obtained for the samples from section S31 are plotted in Figure 24. Although the path followed by the samples from Grimsel has been of sudden wetting (from the initial suction to suction 4 MPa, not shown in the figures) and subsequent drying to suction 120 MPa, it is patent that the evolution of water content experienced by the samples from sections S23 and S31 is in the order of that expected for untreated FEBEX samples of similar initial dry density. The tendency towards a higher retention capacity observed in the samples from Grimsel can be accounted for by hysteresis, since the water content for a given suction is higher in a drying after wetting path than in a wetting path (Villar 2002, Villar *et al*. 2002b).

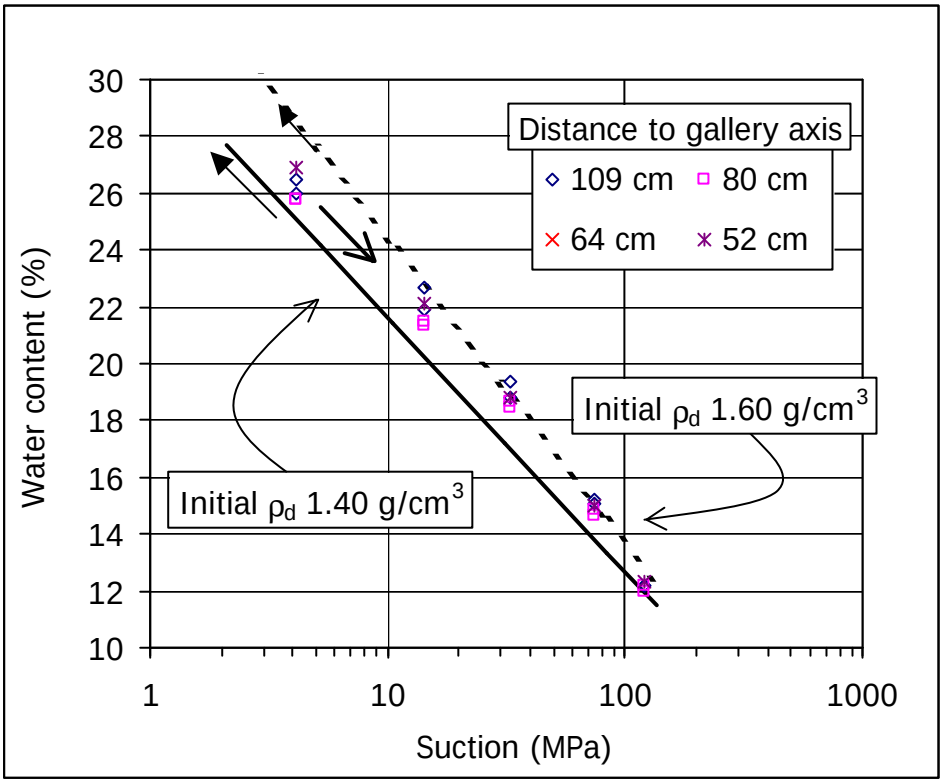

Figure 23: Evolution of water content in a drying path for samples from section S23. The lines correspond to untreated FEBEX bentonite in wetting paths (obtained with Equation 1)

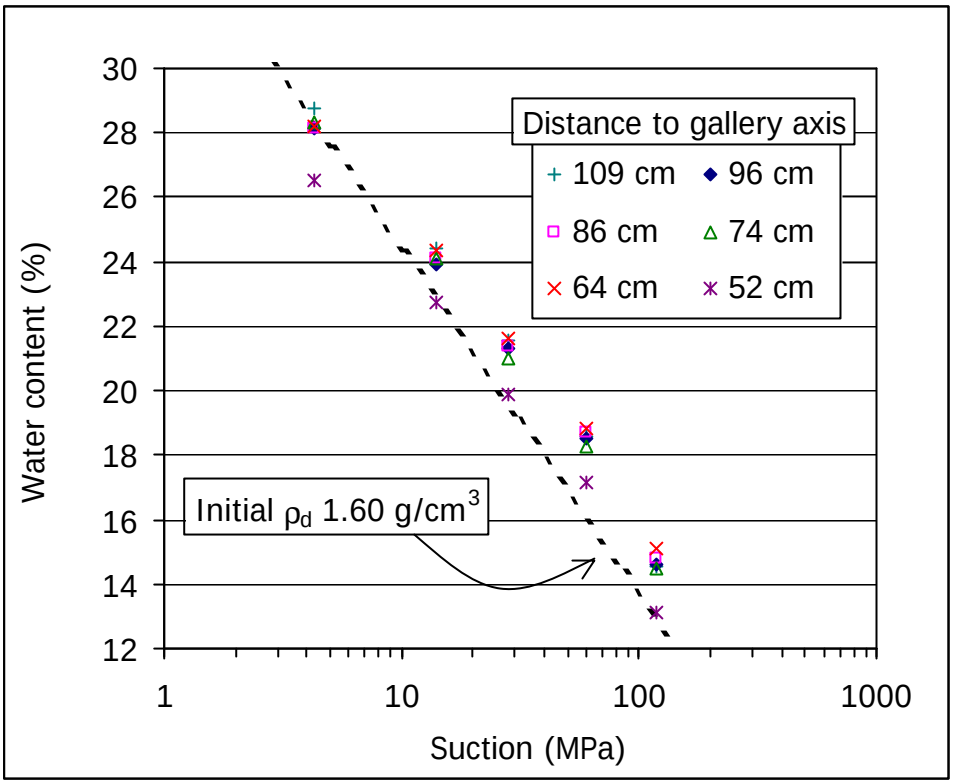

Figure 24: Evolution of water content in a drying path for samples from section S31. The line correspond to untreated FEBEX bentonite in a wetting path (obtained with Equation 1)

On the other hand, the relative humidity of some of the blocks from Grimsel has been measured with capacitive sensors in the laboratory. The plastic and aluminium foil bags were removed and, with the block wrapped in plastic foil, two holes were drilled in it to install the relative humidity sensors inside (Figure 25). When the integrity of the sensor allowed for it, the holes were drilled in external and internal positions with respect to the gallery axis. The transmitters used are ROTRONIC HYGROMETER® CK90, which include a humidity sensor (I-400) that changes its electrical characteristics with extremely small variations in humidity (capacitive type relative humidity sensor). They include also a temperature sensing system (Pt 100). The accuracy of the humidity sensor at 23 °C is ±1.5 percent over the range 0-100 percent *RH*. The clay block-sensors assembly is left for 3-4 hours to stabilise and afterwards the measures are taken. To convert the values of relative humidity (*RH*, %) to suction values (*s*, MPa) the Kelvin's law has been used:

$$s = -10^{-6} \frac{R \times T}{V_w} \ln\left(\frac{RH}{100}\right) \qquad [2]$$

where R is the universal constant of gases (8.3143 J/mol·K), T the absolute temperature and V_w, the molar volume of water ($1.80 \cdot 10^{-5}$ m^3/mol).

Figure 25: Capacitive sensors installed in two different positions of a block from Grimsel

Most of the measurements were performed in August 2003, when the blocks had already been unwrapped and sampled once. This could have given place to modifications of their water contents with respect to the original ones, in fact it seems that there has been an homogenisation of the water content inside the blocks, since the suction measured in different positions are frequently similar. The suction values measured are plotted in Figure 26 as a function of the position in the barrier, indicated as distance to the gallery axis. The values registered by the sensors placed in Grimsel in sections C, E1 and F1 just before the dismantling are also plotted in the figure. There is a good agreement between the measurements taken in the laboratory and those taken *in situ* before dismantling, what corroborates the inertia of the blocks to change their water contents if they are well packed and the reliable performance of the *in situ* instrumentation.

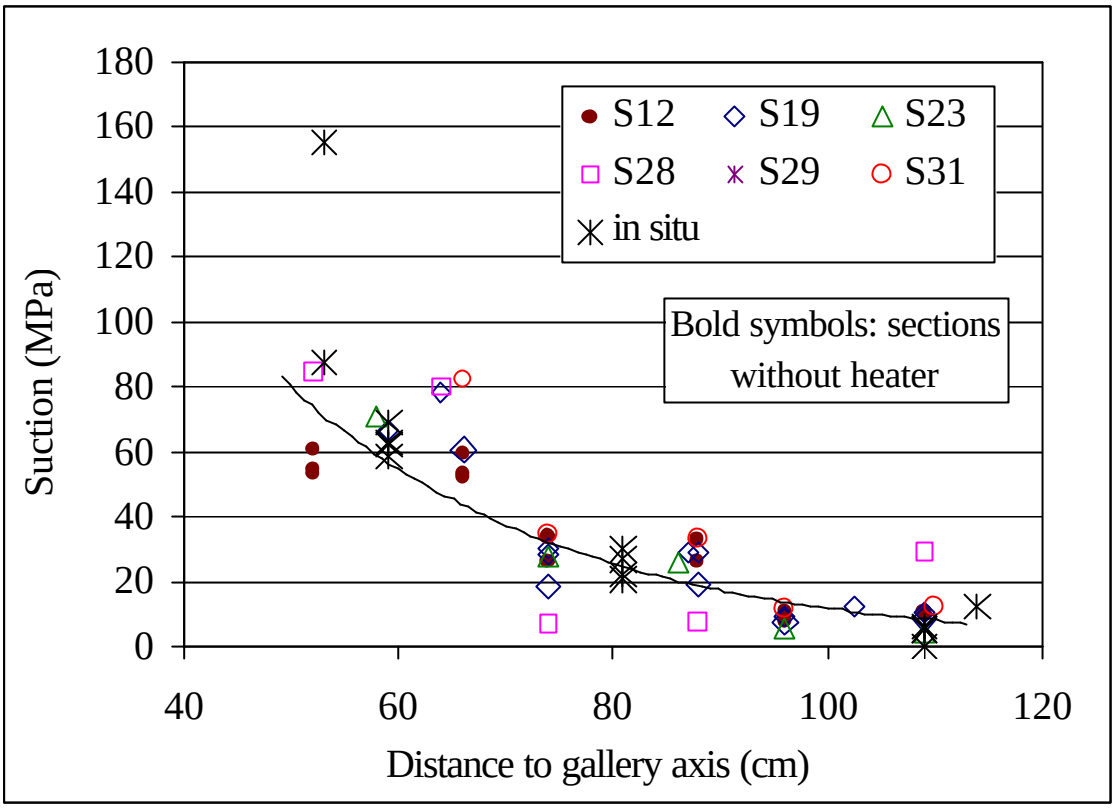

Figure 26: Suction values measured with capacitive sensors *in situ* before dismantling (instrumented sections C (S11), E1 (S21) and F1 (S25)) and in laboratory. The line is a fitting for all the laboratory measurements

The suction values measured in the laboratory have been related to the water contents determined in the same blocks and in the same positions (section 3.2) and are plotted in Figure 27 in the form of a retention curve. The curve determined for untreated FEBEX bentonite compacted at dry density 1.60 g/cm^3 in constant volume cells kept in desiccators with sulphuric acid solutions is also plotted in the figure (Lloret *et al*. in press). This curve was obtained following a wetting path, which is the same process experienced by the samples from Grimsel. The samples with dry density lower than 1.60 g/cm^3 have higher water contents for the same suction than the untreated sample with density 1.60 g/cm^3, whereas the contrary happens for samples of dry density higher, which is the expected trend. Overall, the points obtained in the blocks from Grimsel follow closely the curve for the untreated samples, what suggest that the retention capacity of the FEBEX clay has not changed after five years of being submitted to repository conditions.

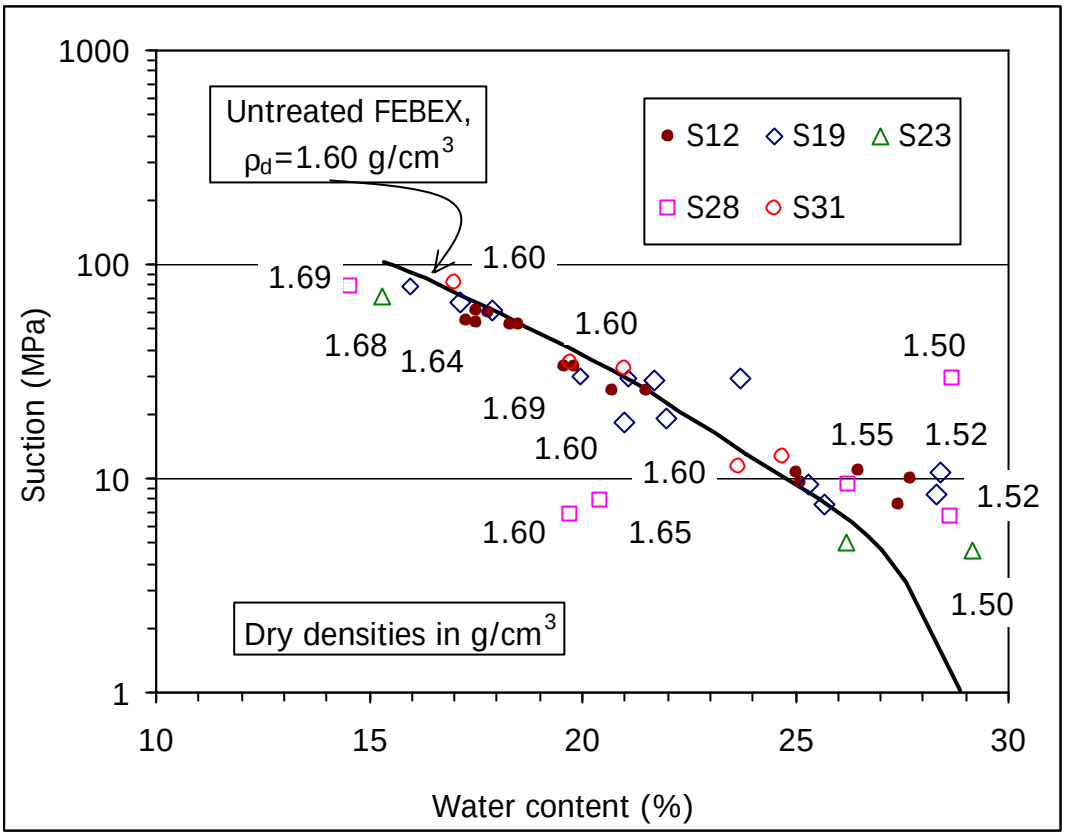

Figure 27: Retention curve as determined from sensor measurements at laboratory in blocks from different sections(points) and determined in untreated FEBEX samples by control of relative humidity at constant volume (line)

3.3.2. Porosimetry

Out of the context of the EC Contract, CIEMAT has performed analysis of pore size distribution by mercury intrusion porosimetry in 25 samples, taken from the sampling sections around the heater S19, S23, S28 and S31, along different radii.

This technique allows the determination of pore size distribution by injecting mercury into the sample at different pressures while controlling the volume intruded. The pressure applied may be related to the minimum pore diameter intruded, taking into account the characteristics of the fluid. The ratio of the volume of mercury intruded (pore volume) to applied pressure (which conditions the minimum pore diameter) allows distribution curves to be obtained establishing the percentage of pores of a size included within a given range.

For this work a Poresizer 9320 porosimeter by Micromeritics was used, with a mercury injection pressure range of 7 kPa to 210 MPa, this allowing pore diameters of between approximately 200 and 0.006 µm to be measured. Consequently, the mercury does not intrude the microporosity (pores of a size of less than 0.002 µm, according to the classification of Sing *et al*. 1985). The mercury intrusion method allows access to be gained only to the macroporosity and to part of the mesopores. Before the samples are inserted in the porosimeter, the water is removed from the pores by freeze-drying. The data obtained are given in accordance with the following key (Tuncer 1988):

– e_1: void ratio calculated from the experimental measurement of specific gravity (with pycnometers: 2.70 g/cm^3) and dry density (by immersion in mercury, see section 3.2).

- e_2: void ratio calculated by mercury intrusion in the porosimeter (or apparent void ratio).
- % total: total percent of pores intruded by mercury.
- ϕ avg. (μm): average pore diameter.
- % large, medium or small: percent of large pores volume (diameter greater than 6 μm), medium-sized pores (diameter between 6 and 0.12 μm) or small pores (diameter between 0.12 and 0.006 μm) with respect to the total volume of intruded pores. This size classification was developed on the basis of porosimetry results obtained from all the clay samples from Grimsel analysed, and includes only macro and mesoporosity. The limits between families may vary slightly between different samples.
- Large, medium or small pore mode (μm).
- unif.coef.: uniformity coefficient of pores ϕ_{40}/ϕ_{80}.

Figure 28 shows a typical porosimetric curve for a sample of untreated FEBEX bentonite compacted at dry density 1.70 g/cm^3 and for two samples taken from Grimsel. The three main families of pores (large, medium and small) may be appreciated in the three samples, the difference among them being the percentage of each family. A summary of the porosimetric data obtained is shown in Table V, in which the results have been grouped according to the position of the samples in the barrier: external, intermediate or inner ring. The results obtained for the untreated FEBEX bentonite compacted at dry density 1.68 g/cm^3 with hygroscopic water content –which are approximately the initial conditions of the blocks placed in Grimsel– are also included in the Table (Villar 2002). Figure 29 shows the distribution of pore sizes obtained for the external, intermediate and internal rings of the barrier and the average distribution for specimens of untreated FEBEX bentonite. The analysis of these results reveals that after being subjected for five years to repository conditions, the bentonite seems to have experienced a redistribution of the size of pores, which is more homogeneous and with a higher average diameter, since the modes of all the pore families have increased. This causes higher uniformity coefficients. There is a relative increase of the percentage of large pores not related to the position of the samples in the barrier. However, the relative percentage of medium pores decreases with respect to the initial one towards the gallery wall, whereas the percentage of small pores decreases with respect to the initial one towards the heater. There is also an overall increase of the percentage of the total porosity that is intruded by mercury in the samples from Grimsel, which maybe simply a consequence of the higher porosity of these samples (their dry density is lower) or may imply either a decrease of pores with a size of less than 0.006 μm (equipment access limit), or more probably, an increase of interconnected pores. In any case, the percent of the porosity intruded by the mercury is fairly low, this meaning that there is still an important volume of pores with a size of less than 0.006 μm or not interconnected. Taking this into account, the percentage of pores in each size range may be recalculated, the merely illustrative average values shown in Table VI being obtained.

The final interpretation of these results must be done taking into account the differences in the dry density and water content of the samples: the dry density of the samples from Grimsel is lower than that of the untreated sample considered, whereas the water contents are higher. The overall increase of volume experienced by the samples at the barrier (which implies a decrease of dry density from that of the compacted blocks –1.70 g/cm^3– to the average density of the barrier –1.58 g/cm^3–, see section 3.2) is probably responsible of the increase of big pores.

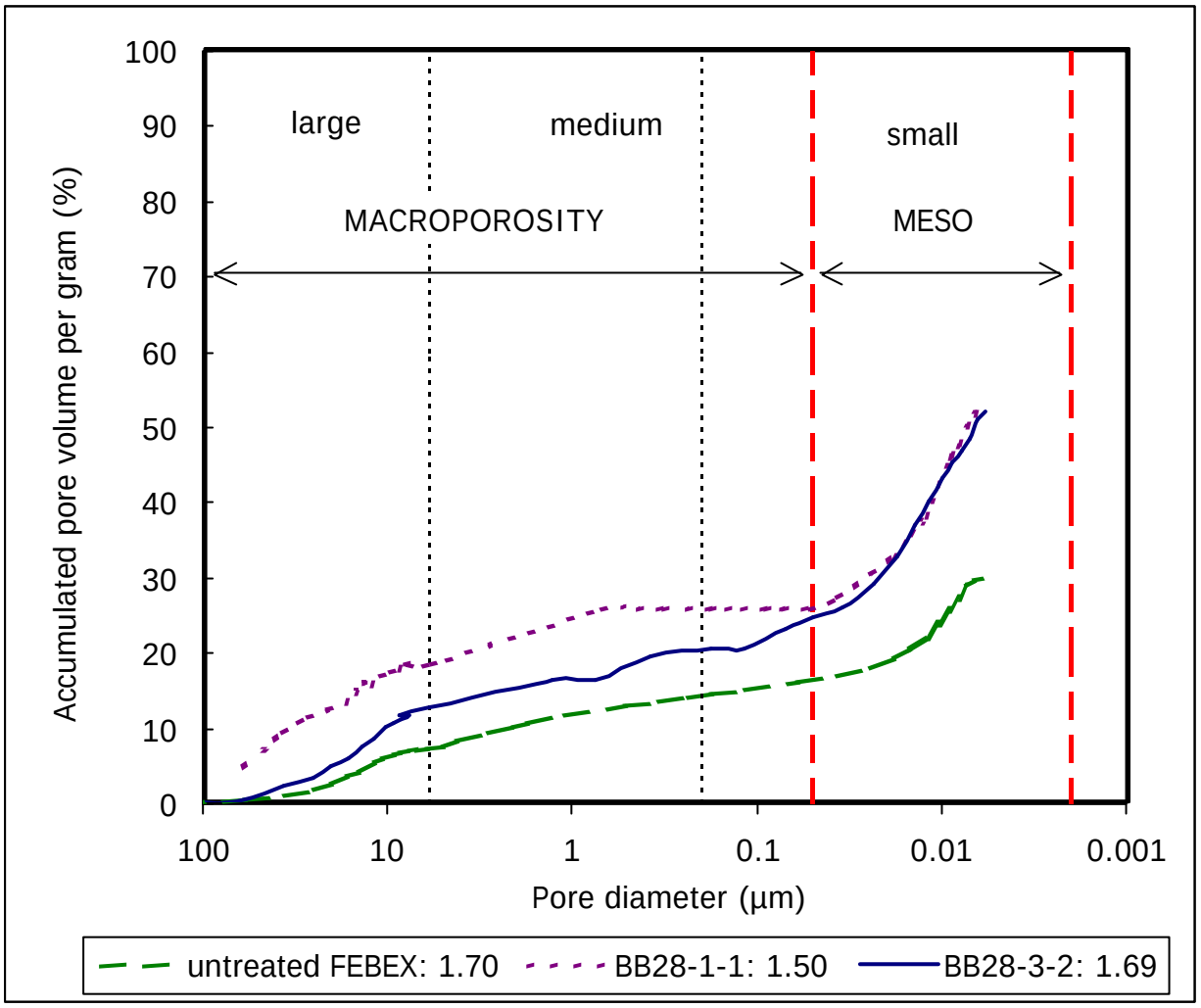

Figure 28: Accumulated porosimetric curve for untreated FEBEX bentonite and two samples from Grimsel, with indication of dry density in g/cm^3 (the percentages are recalculated according to the percentage of total porosity actually intruded by mercury)

Table V: Data on porosimetry by mercury intrusion in the external, intermediate and inner rings of the bentonite barrier and for the untreated FEBEX bentonite

	EXTERNAL	INTERM.	INNER	UNTREATED
No. of samples	8	9	9	15
Water content (%)	26±2	20±1	16±1	14±1
r_d (g/cm^3)	1.55±0.04	1.62±0.02	1.65±0.03	1.68±0.19
e_1	0.748±0.049	0.666±0.019	0.635±0.031	0.640±0.281
e_2	0.400±0.099	0.364±0.032	0.359±0.090	0.193±0.088
% total	54±16	55±6	56±12	34±17
Avg. diameter (µm)	0.02±0.00	0.04±0.03	0.03±0.01	0.02±0.02
% large	28±6	29±4	27±7	23±5
Mode large (µm)	42±4	36±16	38±19	20±12
% medium	16±3	19±3	22±4	22±5
Mode medium (µm)	0.94±0.35	0.83±0.25	0.99±0.35	0.60±0.06
% small	55±7	52±5	51±10	55±6
Mode small (µm)	0.014±0.002	0.014±0.003	0.016±0.003	0.014±0.004
Unif. coef.	145±123	101±73	115±174	44±33

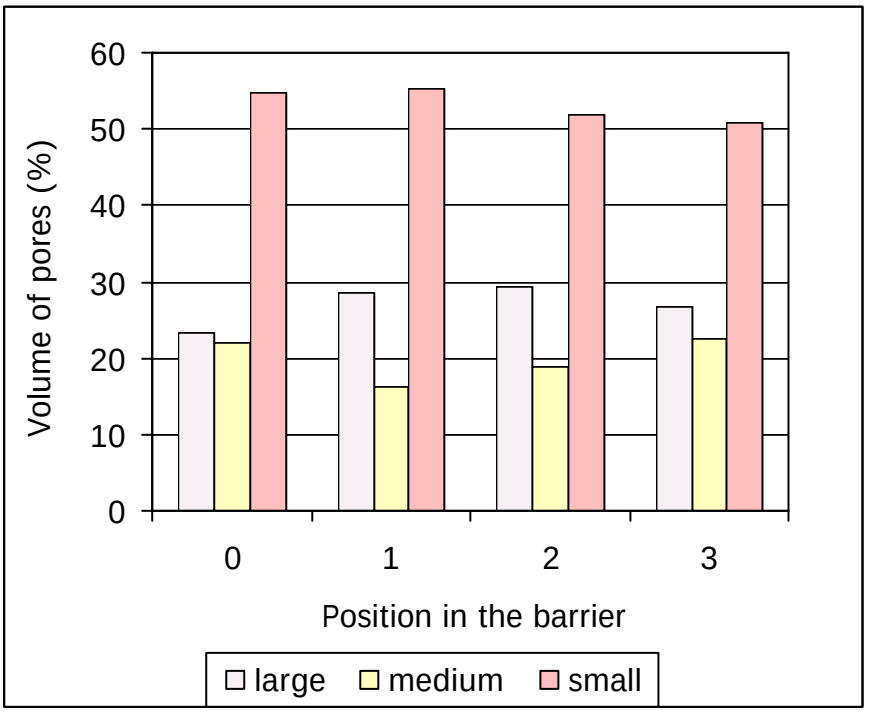

Figure 29: Distribution of large (> 6 µm diameter), medium (between 6 and 0.15 µm) and small (between 0.15 and 0.006 µm) pores in the untreated bentonite compacted at 1.68 g/cm^3 with hygroscopic water content (0), and external (1), intermediate (2) and inner (3) rings of the clay barrier, obtained by mercury intrusion

Table VI: Approximate distribution of total porosity (volume percentage) for samples from Grimsel (external, intermediate and inner rings) and for the untreated FEBEX bentonite (hygroscopic water content, r_d 1.68 g/cm^3)

Size range (µm)	EXTERNAL	INTERM.	INNER	UNTREATED
> 6	15	16	15	7
6 – 0.15	9	10	13	8
0.15 – 0.006	30	28	29	18
< 0.006	46	45	44	67

3.4. TESTS FOR THE STUDY OF WATER FLOW

CIEMAT has determined the hydraulic conductivity of six samples taken from two sections (S19 and S28), at different distances from the heater along a sampling radius. It makes a total of 12 samples: BB19-1A-1, BB19-1A-2, BB19-2A-1, BB19-2A-1, BB19-3A-1, BB19-3A-1, BB28-1A-1, BB28-1A-2, BB28-2A-1, BB28-2A-1, BB28-3A-1, BB28-3A-1.

The theoretical principle on which the method used to determine the hydraulic conductivity is based is that of the fixed load permeameter. Basically, it consists in measuring against time the volume of water that passes through a specimen, confined in a rigid cell preventing it from deforming, to which is applied a constant hydraulic gradient between the upper and lower parts. For this purpose a hydraulic head, that is to say, a difference in potential, is applied between the upper and lower parts of the previously saturated sample. The complete saturation of the sample and associated swelling guarantee perfect contact with the walls of the cell, preventing the flow of water between these and the sample. At the same time, the flow of water passing through the specimen is measured versus time.

The measuring system is made up of the following elements (Figure 30):

- Stainless steel cell with water inlet and outlet, in which the sample is confined.
- Two pressure systems, for injection and downstream pressures. The system used for downstream pressure consists of a set of self-compensating mercury deposits equipped with an installation for deaerated water, whereas for injection pressure Gilson piston pumps (of the type used for high precision liquid chromatography – HPLC) are used.
- Electronic volume change measurement system, with an accuracy of 0.001 cm^3.
- Data acquisition system.

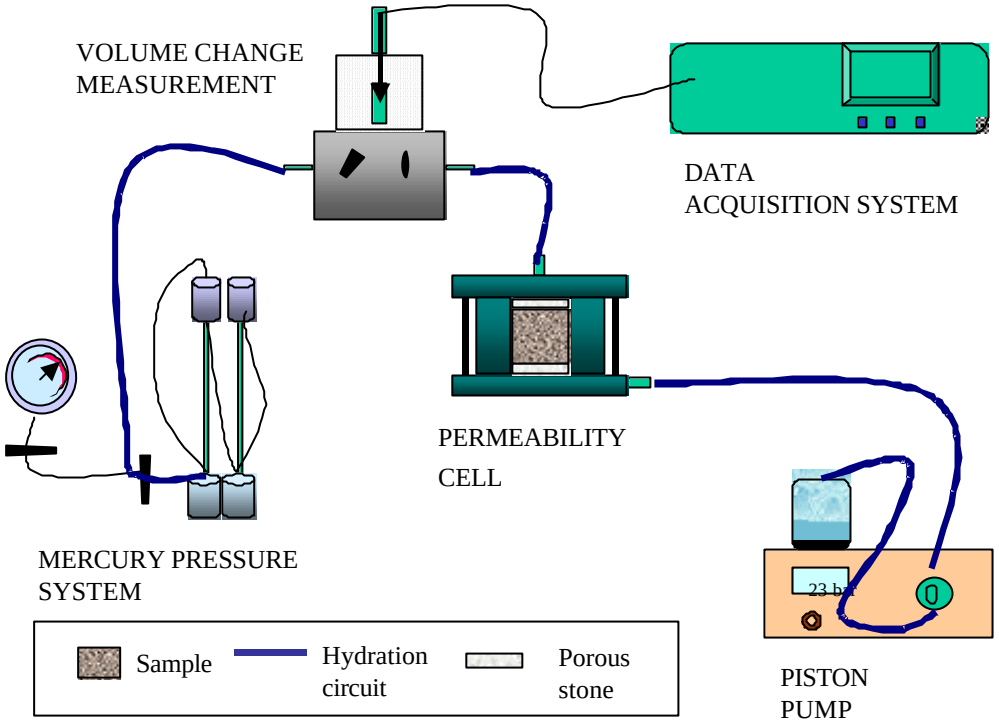

Figure 30: Schematic representation of hydraulic conductivity measuring assembly for expansive soils

The undisturbed samples have been adapted to the diameter of the cell ring by working them with a cylindrical cutter, attempting not to modify either their moisture or density. The nominal dimensions of the sample are 19.63 cm^2 in surface area and 2.50 cm in length. The sample is saturated at 0.6 MPa from both faces with deionised water for a time period usually established at a minimum of two weeks. Once the sample is saturated, the hydraulic gradient is applied by increasing the injection pressure at the lower part of the cell, while the downstream pressure is maintained at 0.6 MPa. The values of hydraulic head applied have ranged from 1.2 MPa to 1.6 MPa, depending on the dry density of the specimen and its permeability. An automatic volume change apparatus is installed between the upper inlet of the cell and the backpressure system. This device is connected to a data acquisition system and periodically records the volume of water passing through the sample. Once constant flow is achieved, permeability is calculated by applying Darcy's law. The determinations have been made at laboratory temperature. The final water content and dry density of the specimen is checked on completion of the test, by drying the sample at 110 °C during 24 hours.

The results obtained are shown in Table VII, in which hydraulic conductivity (k_w) and the initial and final conditions of the samples are indicated. The hydraulic conductivity is clearly related to dry density and the latter in turn is related to the position of the block in the barrier. However, trimming has caused changes in the original dry density of the samples, for which reason dry densities lower than expected are found, particularly in samples from block BB19-2 and BB28-1. It must be pointed out that the values measured do not correspond to the permeability of the bentonite at the moment it was retrieved, since the samples have been saturated to perform the determination, and permeability depends greatly on the degree of saturation. The results are plotted in Figure 31 as a function of the position in the barrier.

Table VII: Results of the hydraulic conductivity determinations performed in samples from section S19 and S28

Block reference	Position[1] (cm)	r_d (g/cm^3)	Initial w (%)	Initial S_r (%)	k_w (m/s)	Final w (%)	Final S_r (%)
BB19-1A-1	109	1.50	29.6	101	$3.3 \cdot 10^{-13}$	31.1	106
BB19-1A-2	96	1.54	26.4	95	$2.3 \cdot 10^{-13}$	29.6	107
BB19-2A-1	88	1.30	23.4	59	$1.9 \cdot 10^{-12}$	41.6	104
BB19-2A-2	74	1.27	22.2	53	$2.8 \cdot 10^{-12}$	44.1	106
BB19-3A-1	66	1.61	18.3	73	$1.7 \cdot 10^{-14}$	27.6	110
BB19-3A-2	52	1.64	16.7	70	$2.2 \cdot 10^{-14}$	26.3	111
BB28-1B-1	109	1.21	29.7	65	$2.4 \cdot 10^{-12}$	47.1	103
BB28-1B-2	96	1.23	28.1	64	$2.3 \cdot 10^{-12}$	46.3	105
BB28-2A-1	88	1.58	21.4	82	$3.9 \cdot 10^{-14}$	28.4	109
BB28-2A-2	74	1.55	20.7	76	$2.4 \cdot 10^{-14}$	30.1	110
BB28-3B-1	66	1.61	14.9	59	$5.6 \cdot 10^{-14}$	28.6	114
BB28-3B-2	52	1.59	15.2	58	$8.3 \cdot 10^{-14}$	27.8	107

[1]Distance to gallery axis

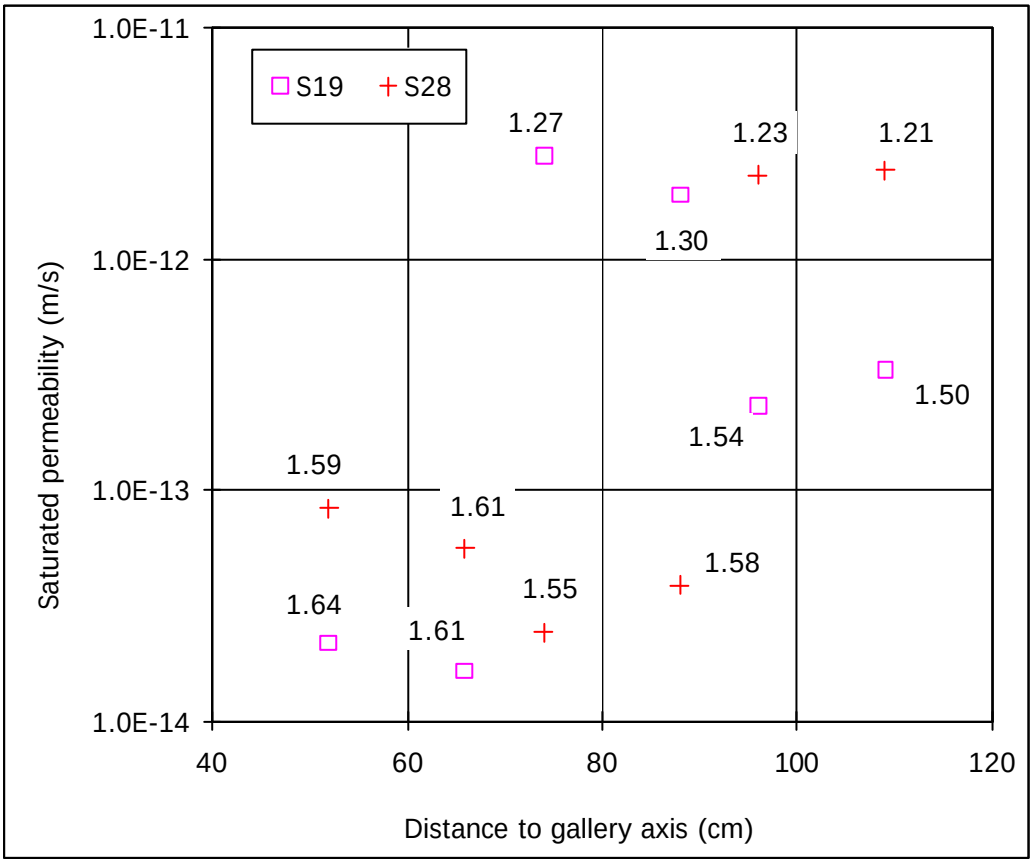

Figure 31: Hydraulic conductivity of samples from sections S19 and S28 (the dry dens ity of the samples is indicated in g/cm^3)

During FEBEX I it was determined the hydraulic conductivity of samples of untreated FEBEX bentonite compacted at different dry densities (Villar 2002). It was found that the values of hydraulic conductivity (k_w, m/s) are exponentially related to dry density (ρ_d, g/cm^3) and a distinction may be made between two different empirical fittings depending on the density interval:

for dry densities of less than 1.47 g/cm^3:

$$\log k_w = -6.00\ \rho_d - 4.09 \qquad (r^2 = 0.97,\ 8 \text{ points}) \qquad [3]$$

for dry densities in excess of 1.47 g/cm^3:

$$\log k_w = -2.96\ \rho_d - 8.57 \qquad (r^2 = 0.70,\ 26 \text{ points}) \qquad [4]$$

The variation in the experimental values with respect to these fittings is smaller for low densities than it is for higher values, with an average –in absolute values– of 30 percent.

These correlations along with the percentage of deviation are plotted in Figure 32 along with the hydraulic conductivities measured in samples from Grimsel. Although the values of hydraulic conductivity for the samples of lower density (more hydrated) are in the order of the theoretical ones, for the higher densities there is a large dispersion without any clear tendency.

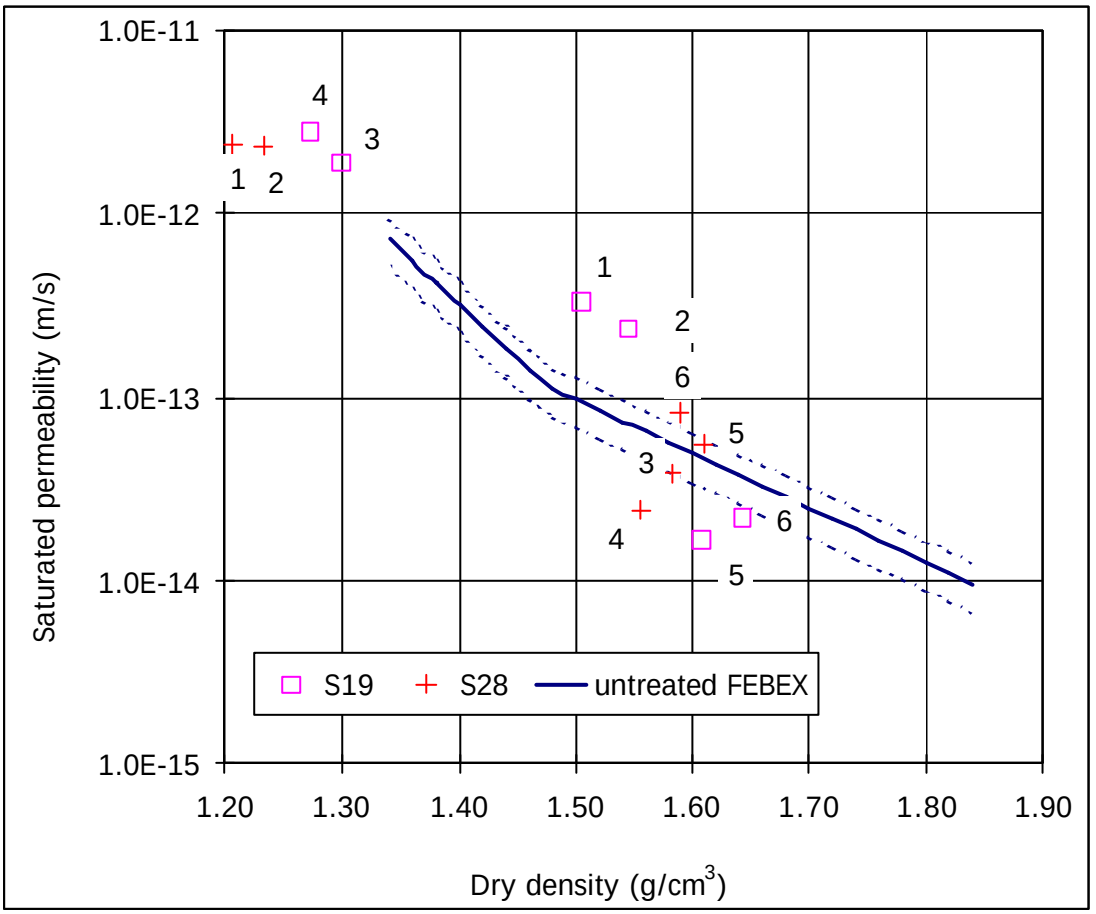

Figure 32: Hydraulic conductivity as a function of dry density for samples of sections S19 and S28. The lines correspond to the empirical fittings obtained with equations 3 and 4 (the position of the samples is indicated with correlative numbers from 1 –closest to gallery wall– to 6 –closest to heater–)

3.5. TESTS TO DETERMINE CHANGES IN THE MECHANICAL PROPERTIES

3.5.1. Swelling deformation tests

The saturation (or swelling) under load test makes it possible to determine the strain capacity of the soil when it saturates under a previously established pressure. Twelve samples, from two different sections (S19 and S28), have been selected to perform this determination, six per section, taken at different distances from the heater along the sampling radii.

The tests have been performed in standard oedometers (Figure 33). Two samples from each block (external and internal position) have been trimmed to the appropriate dimensions (height 1.20 cm, diameter 3.81 cm). For this purpose cylindrical cutters were used, and the samples obtained were placed in the oedometer ring. Once in the oedometer, a vertical pressure of 0.5 MPa has been applied to the samples. Immediately afterwards, the samples are saturated with deionised water at atmospheric pressure from the bottom porous plate. The swelling strain experienced by the specimens upon saturation has been recorded as a function of time until stabilisation. The ratio between the final length increase undergone by the sample in equilibrium with the load applied and its initial length gives the strain value of the material on saturating, the negative values indicating swelling strains. The final result is, therefore, the percentage of strain of a sample of given initial dry density and water content on saturating under a fixed load. On completion of the test, the water content of the specimen was determined by oven drying at 110 °C for 24 hours. The tests have been performed at laboratory temperature.

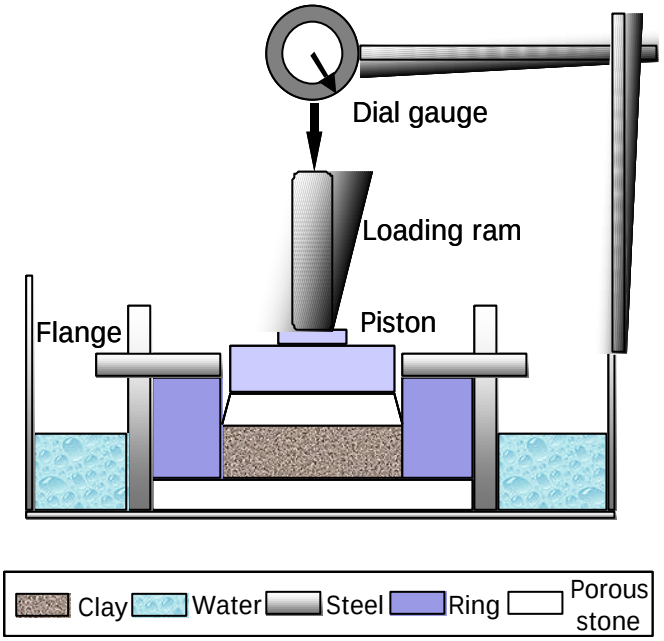

Figure 33: Schematic cross section of an oedometric cell

Table VIII summarises the results of the tests and the initial and final conditions of each sample. Indeed, the samples closer to the gallery wall had higher initial water content and lower initial dry density. The swelling capacity is related to both, increasing with initial dry density and decreasing with initial water content. For this reason the final strain of the samples closer to the heater is higher, as can be clearly seen in Figure 34. The duration of the tests was on average of 20 days. At the end of the tests all the specimens were verified to be completely saturated.

Table VIII: Results of the swelling deformation tests performed in samples from sections S19 and S28

Block reference	Position[1] (cm)	Initial r_d (g/cm^3)	Initial w (%)	Initial S_r (%)	Final strain (%)	Duration (days)	Final w (%)	Final r_d final (g/cm^3)	Final S_r (%)
BB19-1A-1	109	1.48	27.3	90	-9.97	23	38.6	1.35	104
BB19-1A-2	96	1.51	25.4	87	-11.70	23	38.5	1.35	104
BB19-2A-1	88	1.59	24.3	94	-16.18	21	39.8	1.37	111
BB19-2A-2	74	1.52	20.1	70	-11.91	21	37.6	1.36	103
BB19-3A-1	66	1.59	18.9	73	-17.62	16	40.6	1.35	110
BB19-3A-2	52	1.66	16.8	72	-19.94	16	38.5	1.38	109
BB28-1B-1	109	1.45	30.4	95	-6.93	25	37.9	1.36	104
BB28-1B-2	96	1.46	26.0	82	-7.58	25	41.7	1.35	113
BB28-2A-1	88	1.59	21.1	81	-18.09	24	39.6	1.34	106
BB28-2A-2	74	1.67	19.9	87	-18.03	15	37.1	1.41	110
BB28-3B-1	66	1.69	15.6	71	-21.29	14	38.4	1.40	111
BB28-3B-2	52	1.69	9.6	44	-20.82	14	38.3	1.40	112

[1]Distance to gallery axis

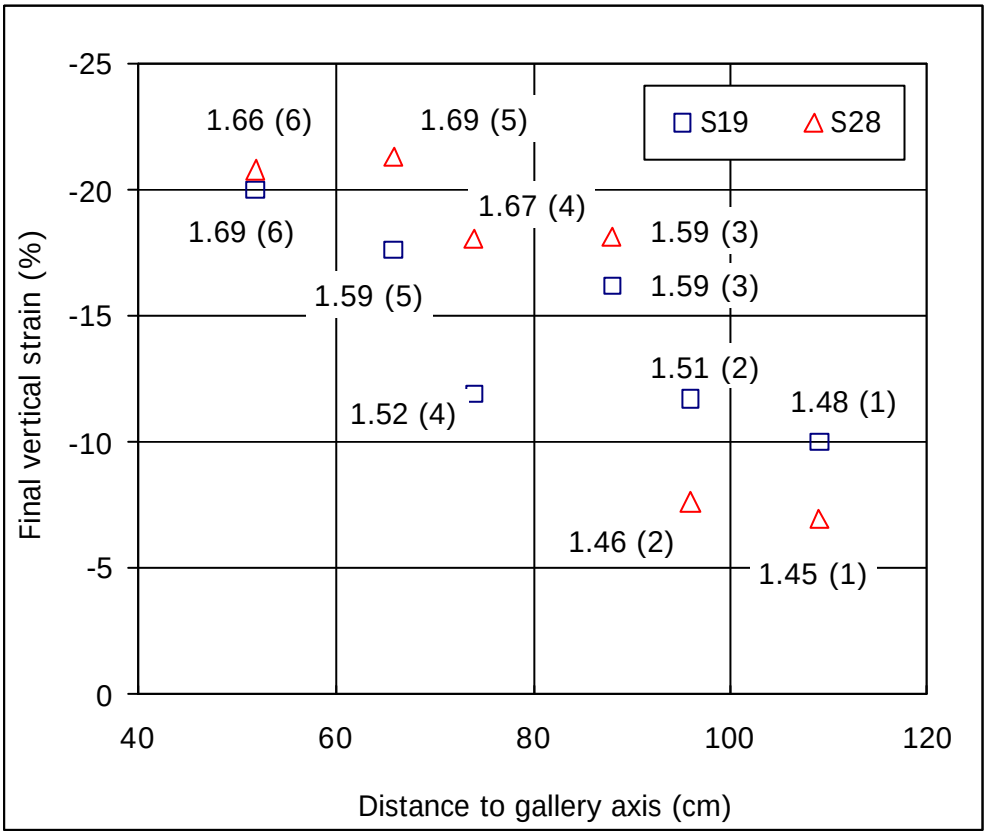

Figure 34: Vertical strain after saturation under 0.5 MPa of samples from sections S19 and S28 (the initial dry density of the samples is indicated in g/cm^3 and their position by correlative numbers from 1 –close to the gallery wall– to 6 –close to the heater–)

Figure 35 and Figure 36 show the evolution of strain versus time in tests performed with specimens of sections S19 and S28, respectively. The figures illustrate how swelling develops more rapidly in the samples of higher initial dry density (and lower initial water content), which correspond to internal positions of the barrier. Their higher suction maybe the explanation of this behaviour.

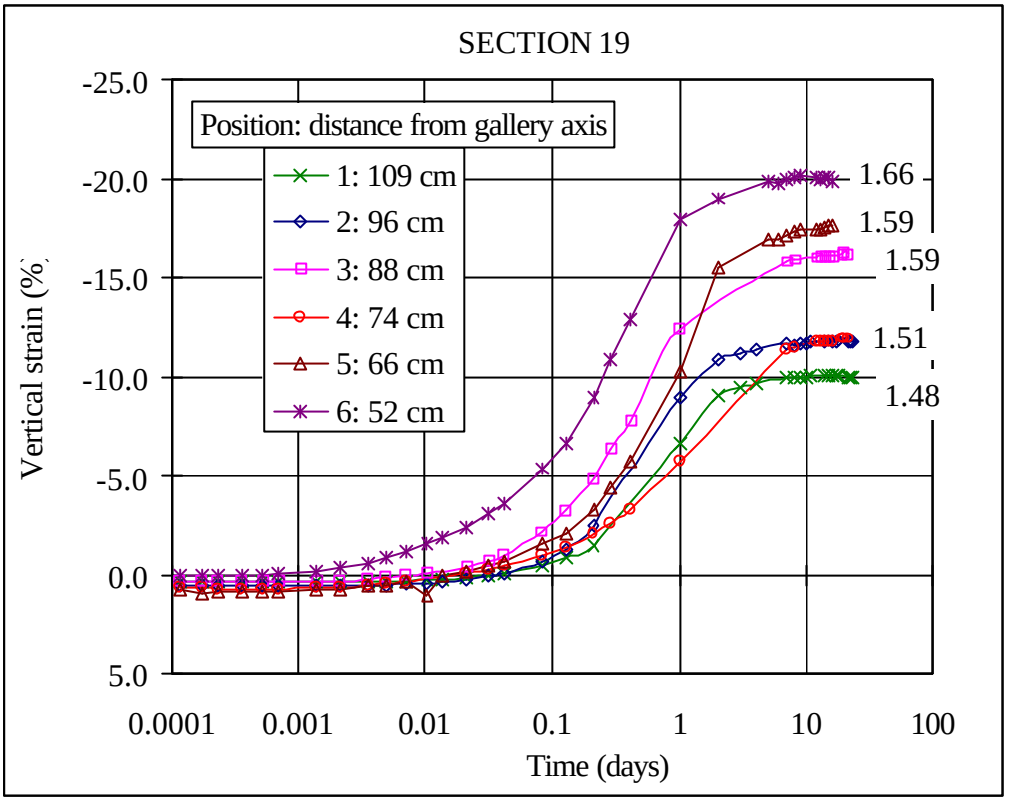

Figure 35: Evolution of vertical strain during saturation under vertical load 0.5 MPa for samples from section S19 (the initial dry density of the samples is indicated in g/cm^3)

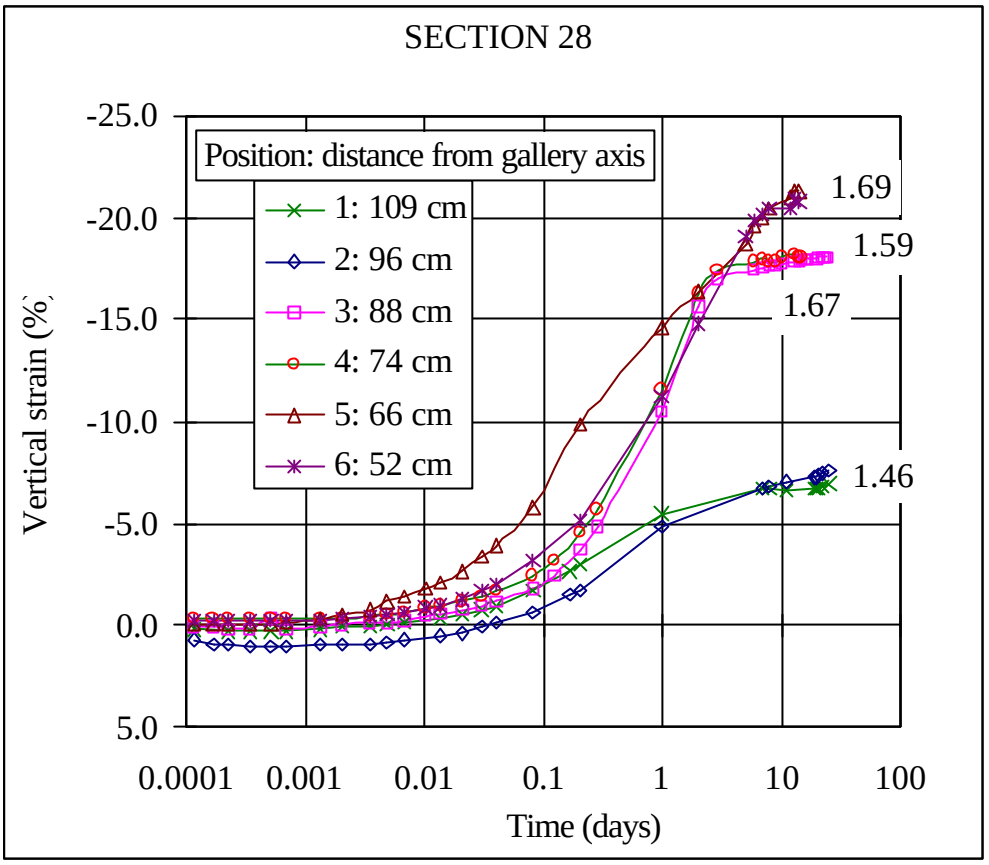

Figure 36: Evolution of vertical strain during saturation under vertical load 0.5 MPa for samples from section S28 (the initial dry density of the samples is indicated in g/cm^3)

Similar tests were performed with samples of untreated FEBEX bentonite compacted at various dry densities with different water contents (Villar *et al*. 2002b). These tests were performed with the aim of having a database with which compare the results presented above. From the results obtained an empirical relation was found between swelling strain (ε, %), initial dry density (ρ_d, g/cm^3), initial water content (w, %) and vertical pressure (σ, MPa), whose predicting capacity is rather good:

$$\varepsilon = [(-12.12 \ln \rho_d + 1.89) \ln \sigma + (36.81 \rho_d - 53.59)] \ln w + (38.27 \ln \rho_d - 1.25) \ln \sigma + (-149.05 \rho_d + 211.42) \quad [5]$$

The results obtained with the samples from sections S19 and S28 are plotted again in Figure 37 as a function of the initial water content of the samples. The figure shows also the theoretical lines obtained with Equation 5 for three different initial dry densities. It can be observed that the final swelling strains of the samples coming from Grimsel are in the order of those expected for the untreated FEBEX bentonite compacted at the same initial dry density with the same water content. This can be clearly seen in Figure 38, in which the values actually measured and the theoretical values obtained with Equation 5 are compared. Consequently, it can be claimed that the swelling capacity of the FEBEX bentonite has not irreversibly changed after five years of being subjected to repository conditions.

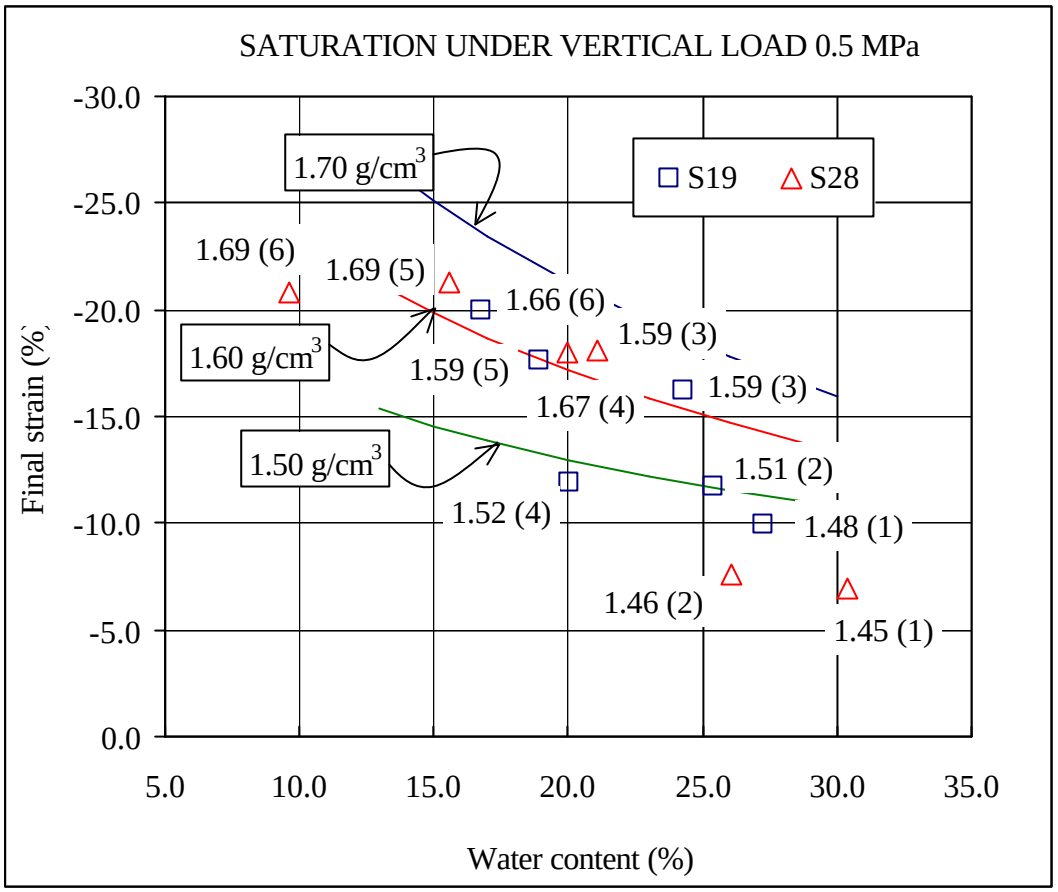

Figure 37: Final strain reached in soaking tests under a vertical pressure of 0.5 MPa for samples of sections 19 and 28. The lines correspond to the empirical fittings obtained with Equation 5 (the initial dry density of the samples is indicated in g/cm³ and their positions with correlative numbers from 1 – closest to gallery wall– to 6 –closest to heater–)

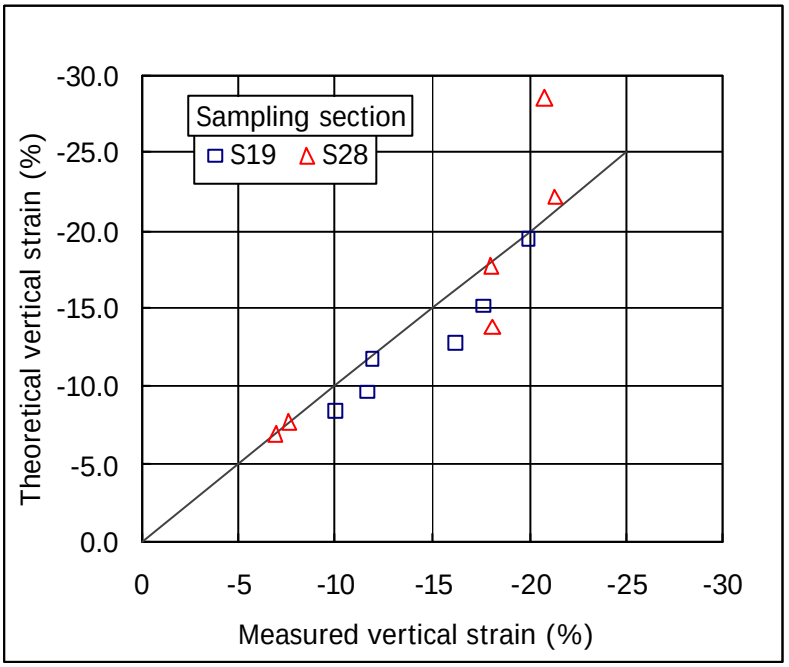

Figure 38: Final strain reached in soaking tests under a vertical pressure of 0.5 MPa compared to the theoretical value obtained with Equation 5

3.5.2. Determination of preconsolidation pressure

The blocks installed in the FEBEX *in situ* test at Grimsel were manufactured by applying uniaxial vertical pressures of between 40 and 45 MPa (ENRESA 2000), which would correspond approximately to the preconsolidation stress of the clay. However, the modification of the structure of the sample –for example as a result of hydration under low load, with which more open structures with higher levels of porosity are obtained–, may cause the value of preconsolidation to decrease. This may be analysed through determination of the preconsolidation pressure (σ'_p) in graphs showing the evolution of void ratio due to increasing load under constant suction. For this reason, the preconsolidation pressure of samples from Grimsel has been determined under oedometric conditions and control of suction.

Twelve samples from two different sections (S19 and S28) have been tested, six per section, taken at different distances from the heater along one sampling radius. The sampled radii chosen are different to those sampled for the strain at saturation tests, consequently, the samples taken are BB19-10-1, BB19-10-2, BB19-11-1, BB19-11-1, BB19-12-1, BB19-12-1, BB28-7A-1, BB28-7A-2, BB28-8A-1, BB28-8A-1, BB28-9A-1, BB28-9A-1. The water content and dry density of the adjacent clay is checked, and the samples are tested under the suction corresponding to that water content according to the water retention curves (Lloret *et al*. in press). Suction is set by means of sulphuric acid solutions. The sample equilibrates at the target suction under a low vertical load. Afterwards, the sample is loaded progressively up to 2, 4, 6, 12 and 20 MPa. The duration of each loading step is fixed to 7 days. The tests have been performed at laboratory temperature.

To perform these tests the oedometric cells of Figure 39 have been adapted to withstand the high pressure supplied by an oedometric frame equipped with a load cell (Figure 40). Cylindrical samples of height 1.2 cm and diameter 3.8 cm are drilled in the bentonite blocks, trimmed if necessary and placed in the oedometer ring. The vertical deformation of the specimen during the test is measured by two LVDTs.

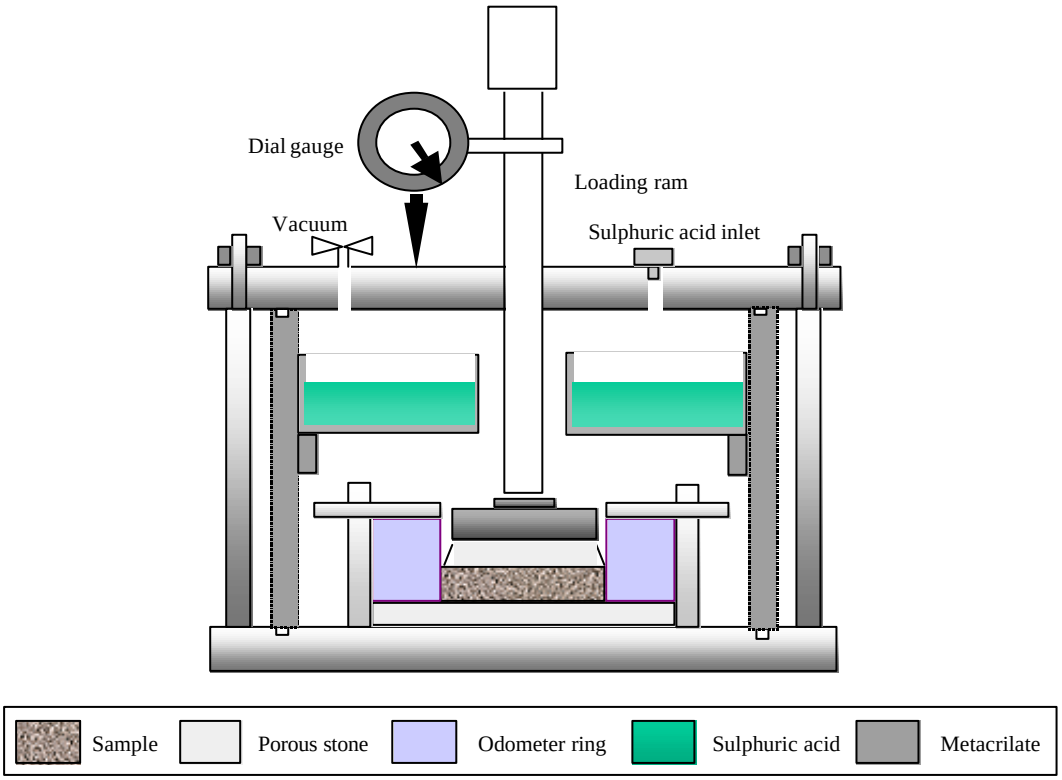

Figure 39: Schematic cross section of an oedometric cell with deposit for solutions

Figure 40: Suction controlled oedometer cells installed in the frames to perform high pressure consolidation tests

In the tests for block BB19-12 each step has been prolonged up to strain stabilisation, instead of being ended after seven days as it was initially foreseen. The initial dry density (ρ_d) and water content (w) of each sample and the corresponding suction are shown in Table IX. The results obtained are shown in Table X to Table XXI. The consolidation curves are shown in Figure 41 to Figure 52 and the oedometric curves in Figure 53 for samples of section S19 and in Figure 54 for samples of section S28. In these figures it can be observed that the preconsolidation pressure is for all the samples lower than 10 MPa, and consequently has decreased with respect to the initial one, the volume increase experienced by the bentonite during hydration accounting for that. Furthermore, the preconsolidation stresses found are lower the lower the suction applied during the test, *i.e*. the higher the water content reached during the *in situ* experiment. These values are plotted as a function of suction in Figure 55, in which the apparent preconsolidation stresses found for samples of untreated FEBEX bentonite compacted initially to similar dry densities and subjected to different suctions are also shown (Villar 2002, Lloret *et al*. 2002). The latter values correspond to consolidation of samples initially hydrated under low vertical stresses, and since they have swollen during the wetting more than the Grimsel samples (which are "confined"), their preconsolidation pressures are even lower.

Table IX: Initial conditions of the samples used in the consolidation tests

Sample	Position[1] (cm)	Initial r_d (g/cm^3)	Initial w (%)	Suction (MPa)
BB19-10A-1	109	1.52	28.4	3
BB19-10A-2	96	1.57	25.3	9
BB19-11A-1	88	1.59	23.7	7

Sample	Position[1] (cm)	Initial r_d (g/cm^3)	Initial *w* (%)	Suction (MPa)
BB19-11A-2	74		21.7	35
BB19-12A-1	66	1.64	17.8	67
BB19-12A-2	52	1.65	16.5	84
BB28-7A-1	109	1.54	27.9	2
BB28-7A-2	96	1.54	25.8	7
BB28-8A-1	88	1.63	21.0	27
BB28-8A-2	74	1.57	20.0	30
BB28-9A-1	66	1.69	14.4	104
BB28-9A-2	52	1.74	15.6	132

[1] Distance to gallery axis

Table X: Results of the consolidation test in sample BB19-10A-1 (external ring), performed unde r suction 3 MPa

STEP	Initial r_d (g/cm^3)	Vertical pressure (MPa)	Final r_d g/cm^3)	Final *e*	Duration (days)
0	1.54	0.3	1.53	0.765	7
1	1.53	1.6	1.54	0.758	7
2	1.54	3.2	1.55	0.745	13
3	1.55	7.1	1.58	0.712	7
4	1.58	10.6	1.68	0.611	7
5	1.68	21.1	1.84	0.471	7

Table XI: Results of the consolidation test in sample BB19-10A-2 (external ring), performed under suction 9 MPa

STEP	Initial r_d (g/cm^3)	Vertical pressure (MPa)	Final r_d g/cm^3)	Final *e*	Duration (days)
0	1.48	0.1	1.48	0.828	7
1	1.48	1.7	1.50	0.804	7
2	1.50	3.3	1.51	0.784	13
3	1.51	7.2	1.56	0.734	7
4	1.56	10.7	1.65	0.632	7
5	1.65	21.2	1.76	0.530	7

Table XII: Results of the consolidation test in sample BB19-11A-1 (intermediate ring), performed under suction 7 MPa

STEP	Initial ρ_d (g/cm^3)	Vertical pressure (MPa)	Final ρ_d g/cm^3)	Final *e*	Duration (days)
0	1.59	1.2	1.60	0.690	4
1	1.60	1.5	1.58	0.707	10
2	1.58	3.2	1.59	0.699	14
3	1.59	7.3	1.61	0.676	8
4	1.61	10.8	1.67	0.613	7
5	1.67	21.3	1.76	0.537	9
6	1.76	35.3	1.90	0.419	7

Table XIII: Results of the consolidation test in sample BB19-11A-2 (intermediate ring), performed under suction 35 MPa

STEP	Initial ρ_d (g/cm^3)	Vertical pressure (MPa)	Final ρ_d g/cm^3)	Final *e*	Duration (days)
0	1.53	0.9	1.54	0.754	4
1	1.54	1.6	1.55	0.746	10
2	1.55	3.2	1.55	0.737	14
3	1.55	7.3	1.57	0.714	8
4	1.57	10.8	1.62	0.666	7
5	1.62	21.4	1.72	0.567	9
6	1.72	35.3	1.87	0.446	7

Table XIV: Results of the consolidation test in sample BB19-12A-1 (internal ring), performed under suction 67 MPa

STEP	Initial ρ_d (g/cm^3)	Vertical pressure (MPa)	Final ρ_d g/cm^3)	Final *e*	Duration (days)
0	1.59	0.9	1.60	0.692	6
1	1.60	1.7	1.60	0.689	4
2	1.60	3.6	1.61	0.677	6
3	1.61	7.1	1.62	0.662	15
4	1.62	10.8	1.72	0.567	18
5	1.72	21.2	1.83	0.475	20
6	1.83	31.3	1.96	0.380	18

Table XV: Results of the consolidation test in sample BB19-12A-2 (internal ring), performed under suction 84 MPa

STEP	Initial ρ_d (g/cm^3)	Vertical pressure (MPa)	Final ρ_d g/cm^3)	Final *e*	Duration (days)
0	1.56	0.6	1.56	0.735	6
1	1.56	1.8	1.56	0.730	4
2	1.56	3.7	1.56	0.726	6
3	1.56	7.1	1.58	0.708	15
4	1.58	10.9	1.65	0.633	18
5	1.65	21.2	1.74	0.549	20
6	1.74	31.4	1.89	0.428	18

Table XVI: Results of the consolidation test in sample BB28-7A-1 (external ring), performed under suction 2 MPa

STEP	Initial ρ_d (g/cm^3)	Vertical pressure (MPa)	Final ρ_d g/cm^3)	Final *e*	Duration (days)
0	1.54	0.4	1.55	0.747	5
1	1.55	1.4	1.54	0.750	8
2	1.54	3.7	1.54	0.748	7
3	1.54	7.1	1.55	0.741	8
4	1.55	10.6	1.60	0.690	7
5	1.60	21.2	1.72	0.569	6
6	1.72	35.4	1.84	0.467	7

Table XVII: Results of the consolidation test in sample BB28-7A-2 (external ring), performed under suction 7 MPa

STEP	Initial ρ_d (g/cm^3)	Vertical pressure (MPa)	Final ρ_d g/cm^3)	Final *e*	Duration (days)
0	1.59	0.5	1.60	0.687	5
1	1.60	1.5	1.60	0.687	8
2	1.60	3.7	1.61	0.682	7
3	1.61	7.1	1.61	0.674	8
4	1.61	10.7	1.67	0.621	7
5	1.67	21.2	1.75	0.546	6
6	1.75	35.4	1.85	0.462	7

Table XVIII: Results of the consolidation test in sample BB28-8A-1 (intermediate ring), performed under suction 27 MPa

STEP	Initial r_d (g/cm^3)	Vertical pressure (MPa)	Final r_d g/cm^3)	Final *e*	Duration (days)
0	1.64	0.4	1.63	0.654	5
1	1.63	1.7	1.64	0.651	8
2	1.64	3.9	1.65	0.640	7
3	1.65	7.9	1.66	0.622	7
4	1.66	11.1	1.72	0.568	8
5	1.72	21.1	1.80	0.498	7
6	1.80	35.0	1.89	0.428	7

Table XIX: Results of the consolidation test in sample BB28-8A-2 (intermediate ring), performed under suction 30 MPa

STEP	Initial r_d (g/cm^3)	Vertical pressure (MPa)	Final r_d g/cm^3)	Final *e*	Duration (days)
0	1.49	0.5	1.49	0.818	5
1	1.49	1.7	1.49	0.813	8
2	1.49	4.0	1.50	0.801	7
3	1.50	7.9	1.52	0.779	7
4	1.52	11.2	1.56	0.731	8
5	1.56	21.2	1.63	0.658	7
6	1.63	35.6	1.70	0.593	7

Table XX: Results of the consolidation test in sample BB28-9A-1 (internal ring), performed under suction 104 MPa

STEP	Initial r_d (g/cm^3)	Vertical pressure (MPa)	Final r_d g/cm^3)	Final *e*	Duration (days)
0	1.61	0.3	1.61	0.677	8
1	1.61	2.5	1.64	0.649	11
2	1.64	4.1	1.64	0.642	7
3	1.64	7.7	1.66	0.626	8
4	1.66	11.1	1.69	0.599	7
5	1.69	20.5	1.75	0.540	9
6	1.75	35.5	1.85	0.458	7

Table XXI: Results of the consolidation test in sample BB28-9A-2 (internal ring), performed under suction 132 MPa

STEP	Initial r_d (g/cm^3)	Vertical pressure (MPa)	Final r_d g/cm^3)	Final *e*	Duration (days)
0	1.68	0.2	1.69	0.599	8
1	1.69	2.6	1.72	0.573	11
2	1.72	4.2	1.72	0.567	7
3	1.72	7.8	1.74	0.551	8
4	1.74	11.1	1.80	0.502	7
5	1.80	20.8	1.86	0.454	9
6	1.86	35.3	1.95	0.384	7

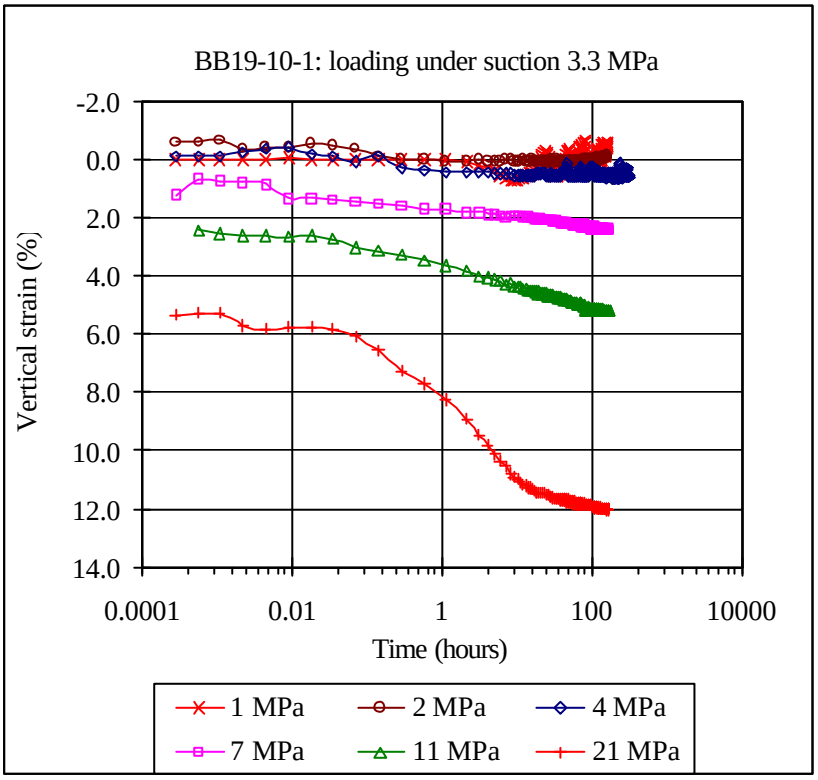

Figure 41: Evolution of strain during the different steps of the process of loading under suction 3 MPa for sample BB19-10A-1

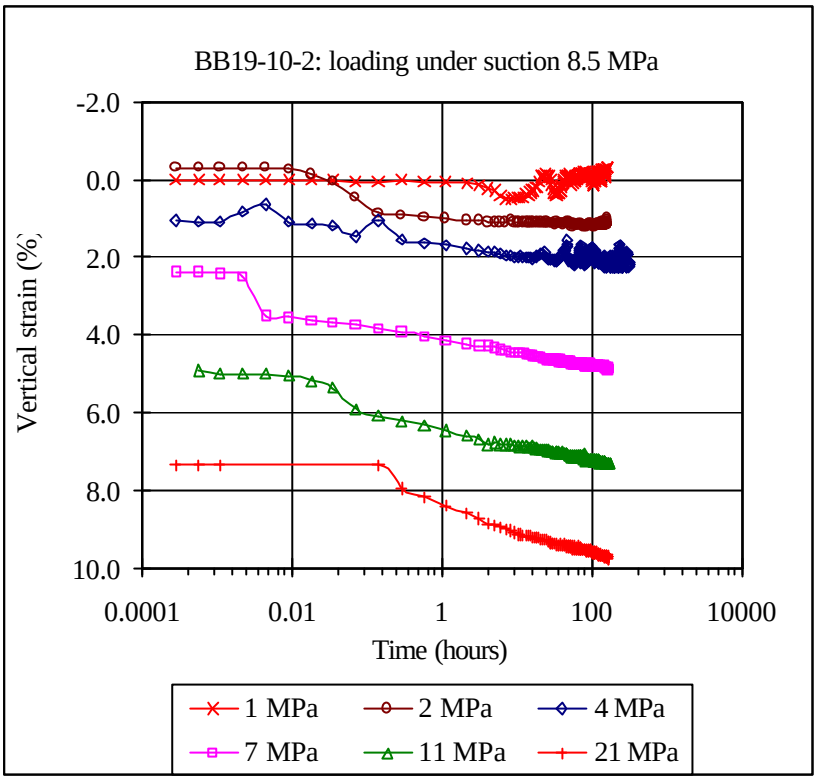

Figure 42: Evolution of strain during the different steps of the process of loading under suction 9 MPa for sample BB19-10A-2

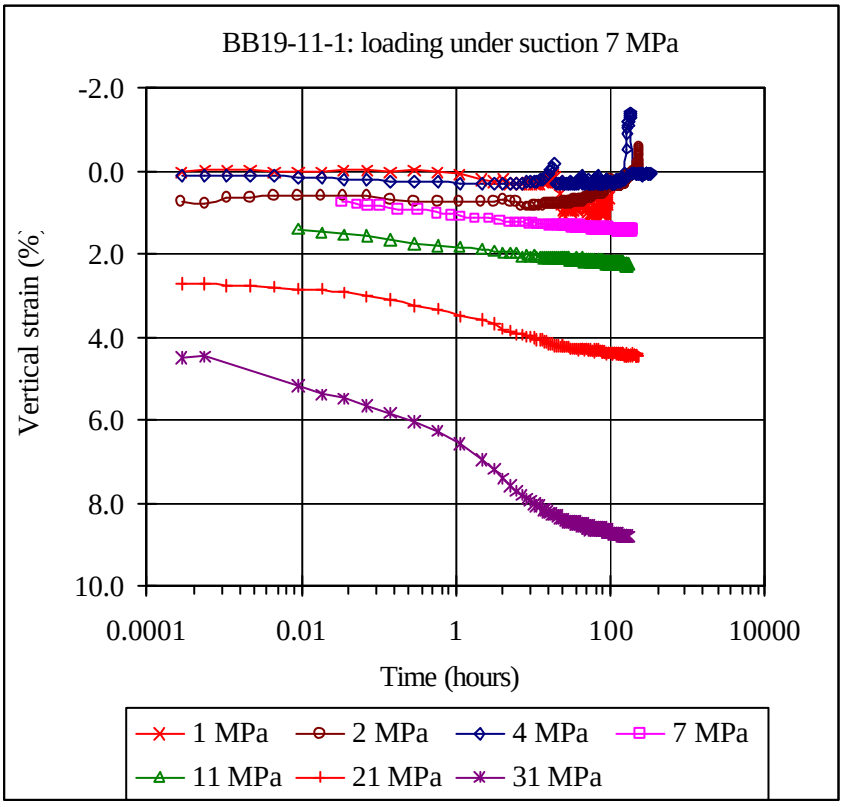

Figure 43: Evolution of strain during the different steps of the process of loading under suction 7 MPa for sample BB19-11A-1

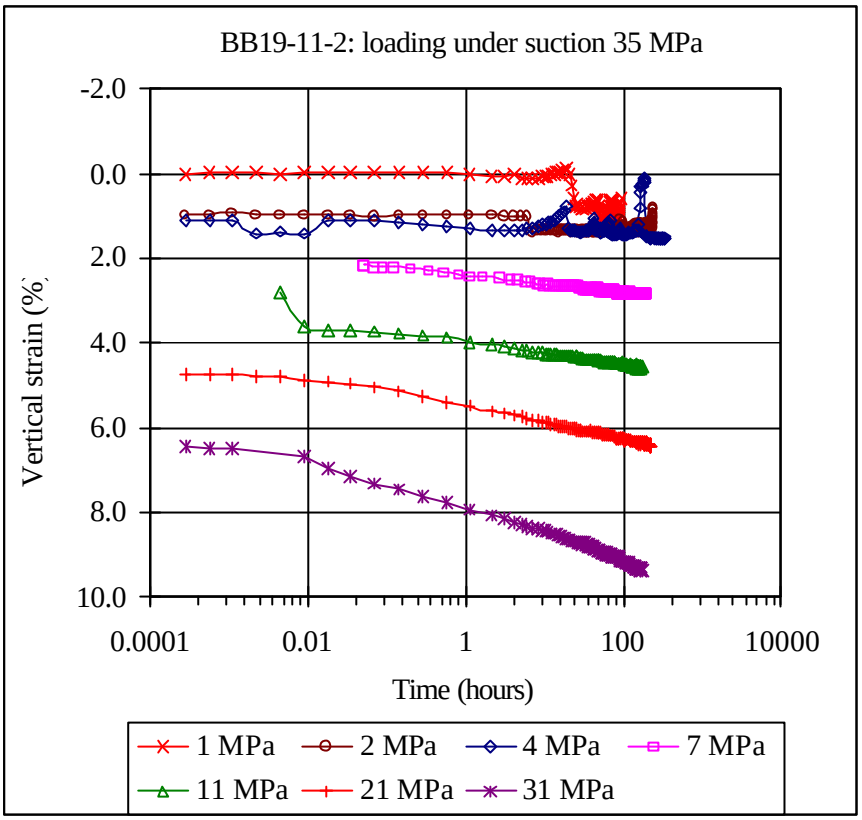

Figure 44: Evolution of strain during the different steps of the process of loading under suction 35 MPa for sample BB19-11A-2

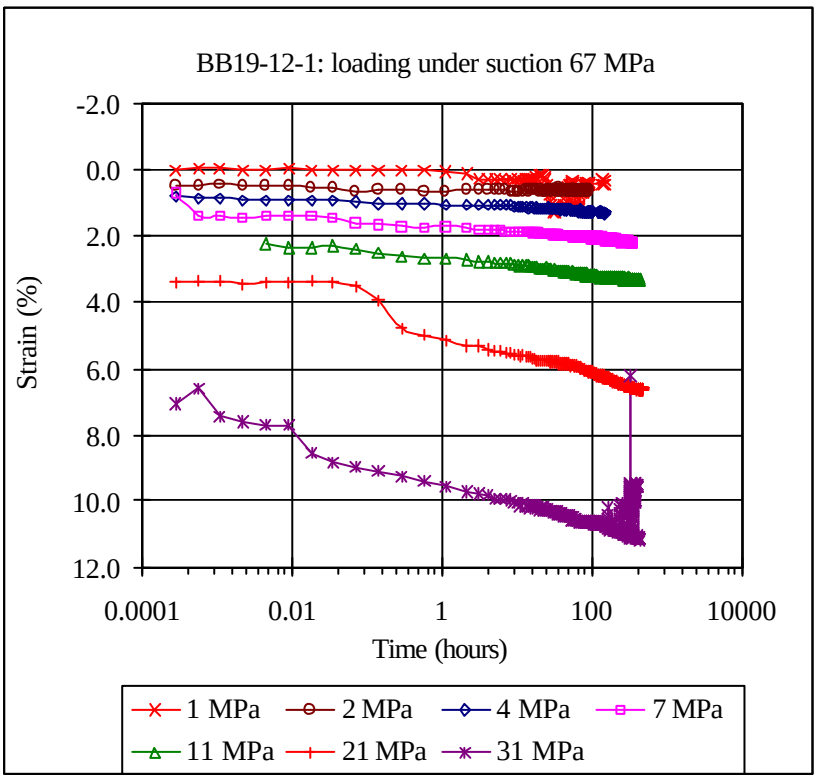

Figure 45: Evolution of strain during the different steps of the process of loading under suction 67 MPa for sample BB19-12A-1

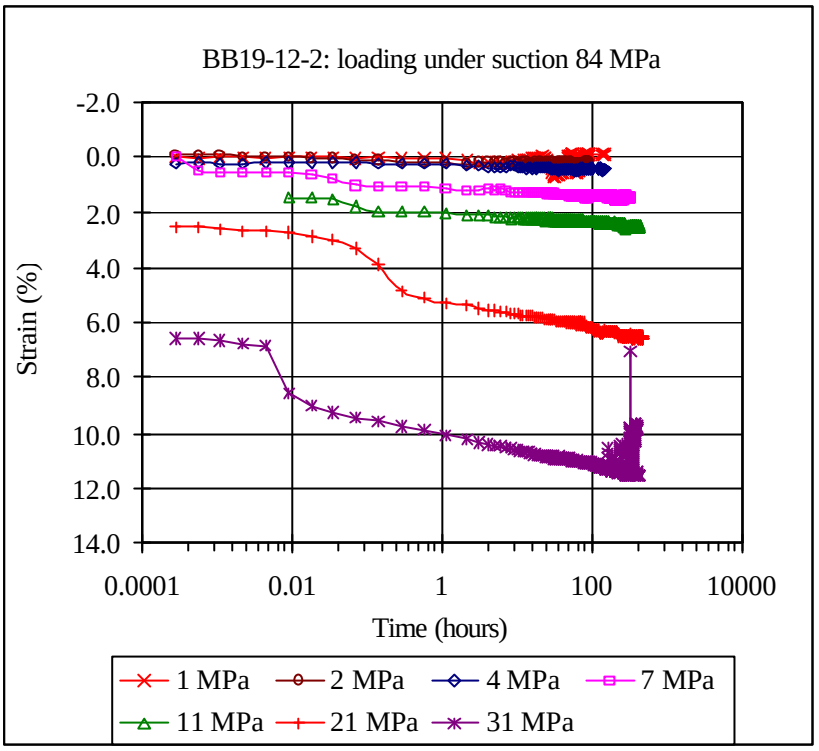

Figure 46: Evolution of strain during the different steps of the process of loading under suction 84 MPa for sample BB19-12A-2

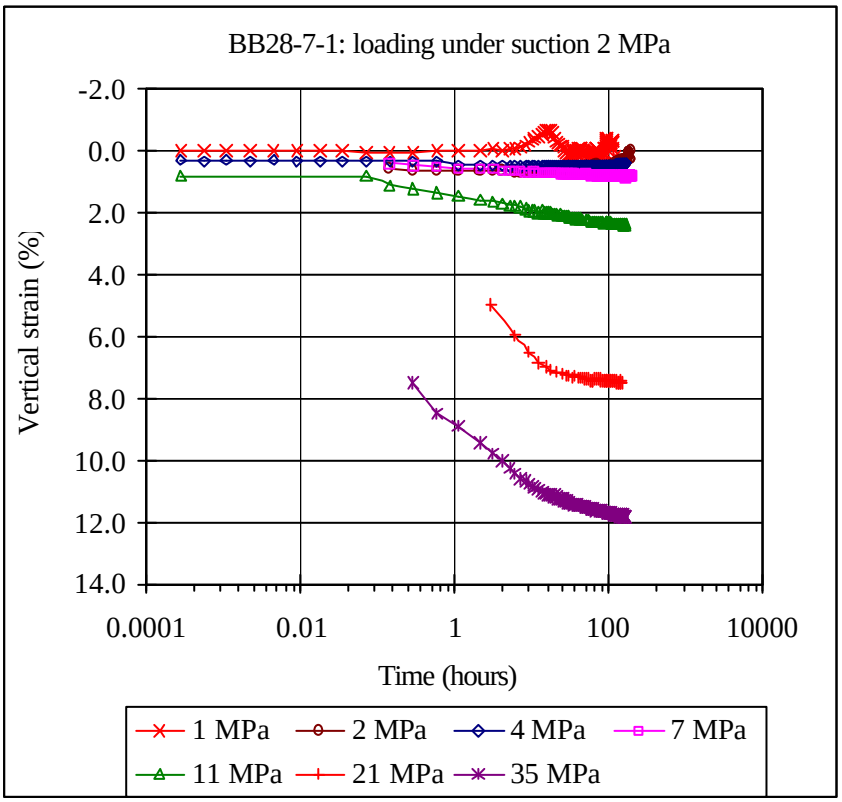

Figure 47: Evolution of strain during the different steps of the process of loading under suction 2 MPa for sample BB28-7A-1

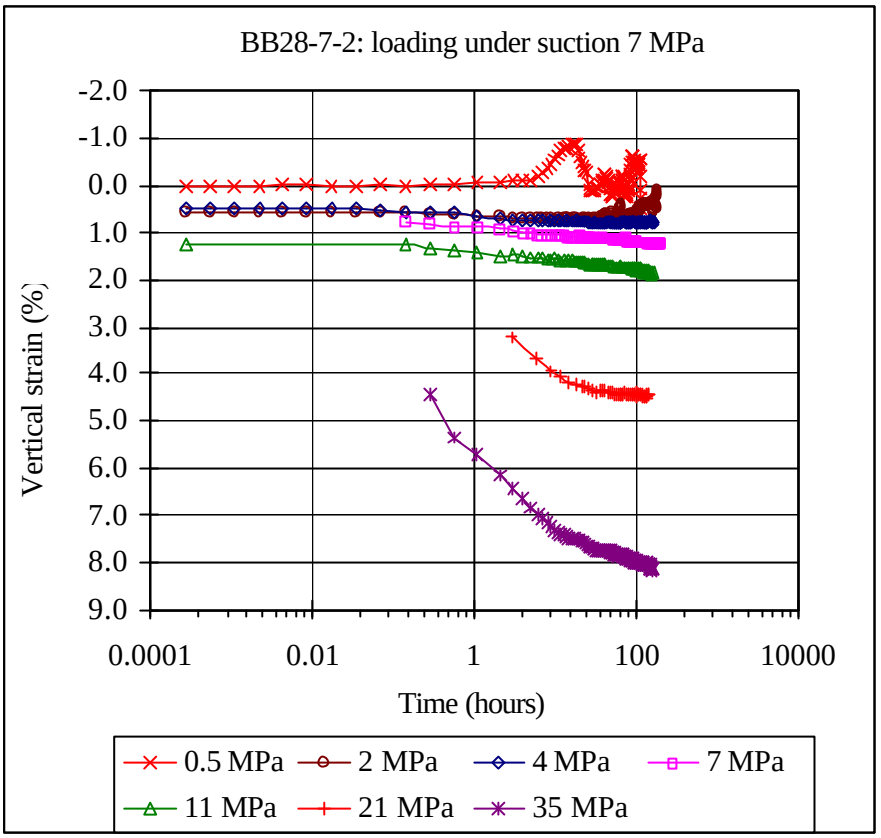

Figure 48: Evolution of strain during the different steps of the process of loading under suction 7 MPa for sample BB28-7A-2

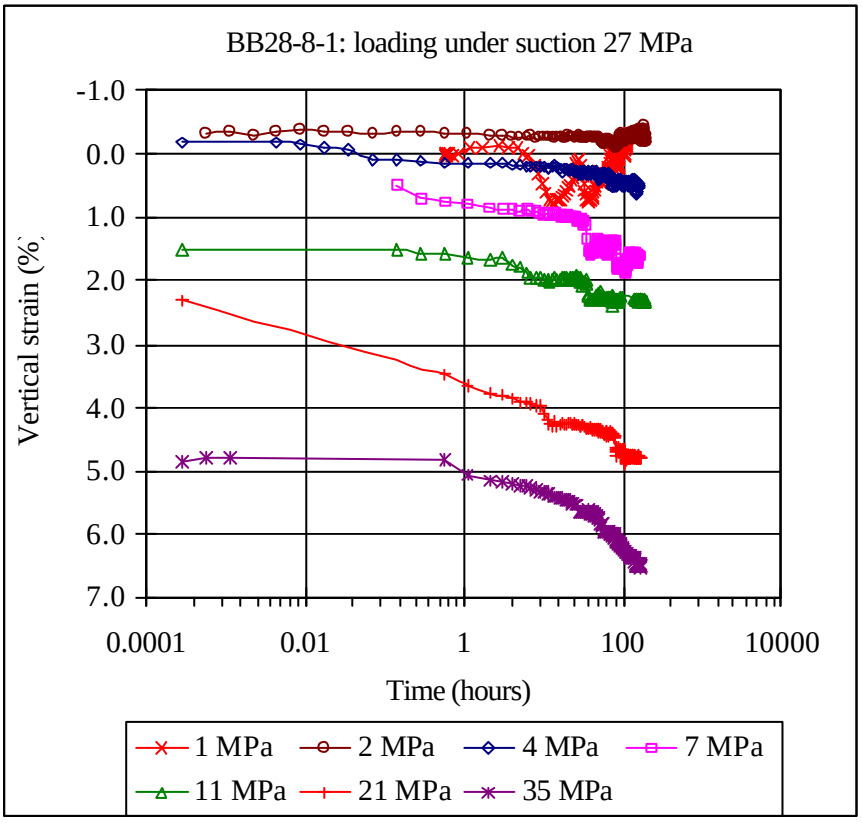

Figure 49: Evolution of strain during the different steps of the process of loading under suction 27 MPa for sample BB28-8A-1

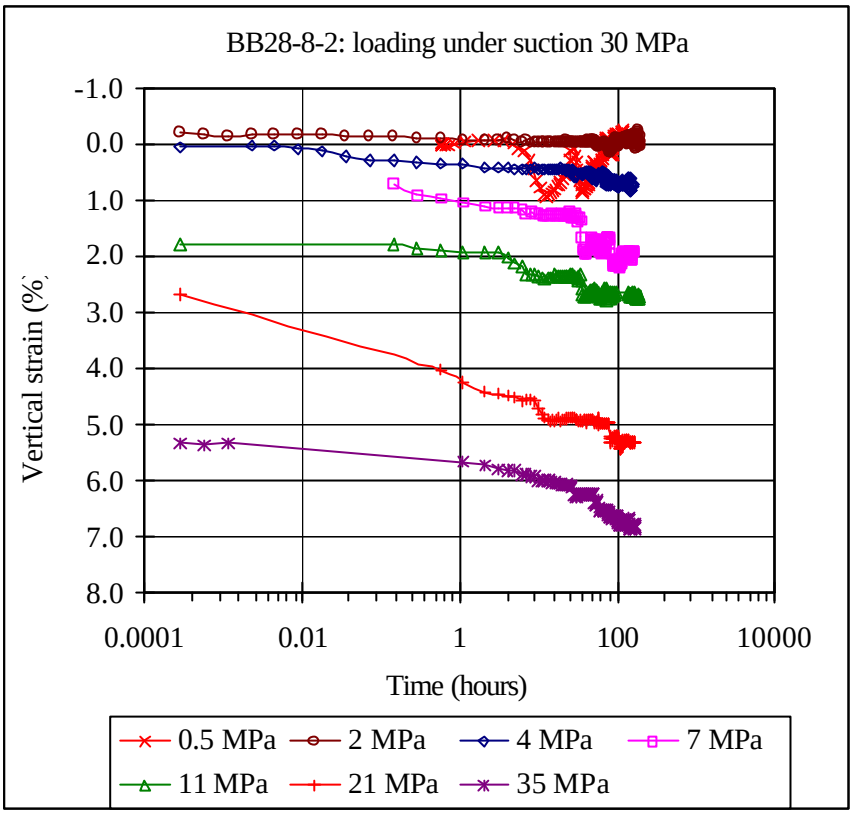

Figure 50: Evolution of strain during the different steps of the process of loading under suction 30 MPa for sample BB28-8A-2

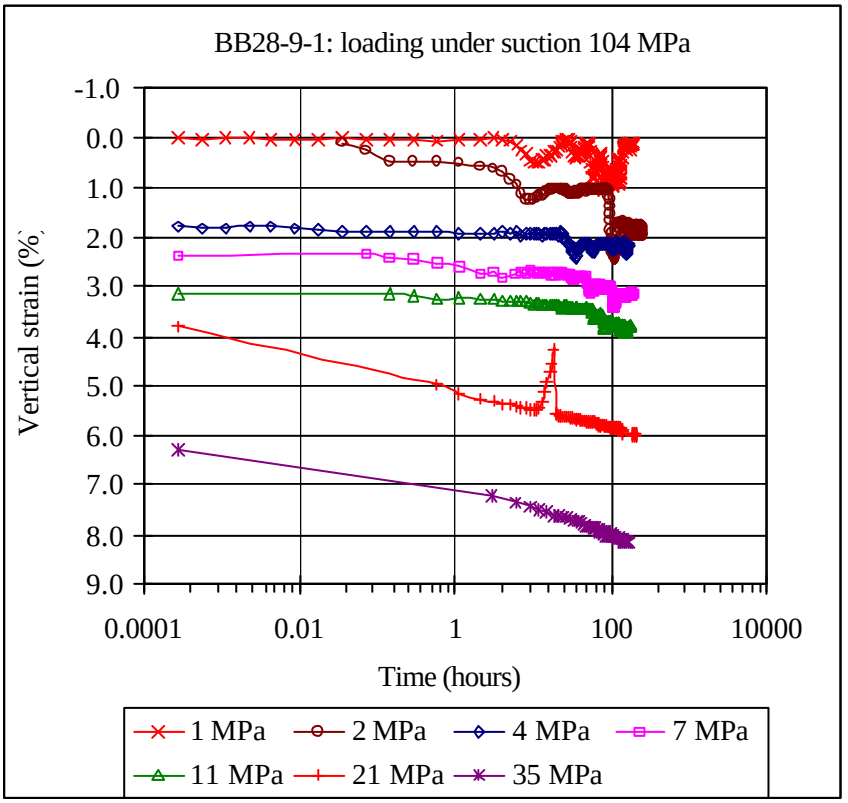

Figure 51: Evolution of strain during the different steps of the process of loading under suction 104 MPa for sample BB28-9A-1

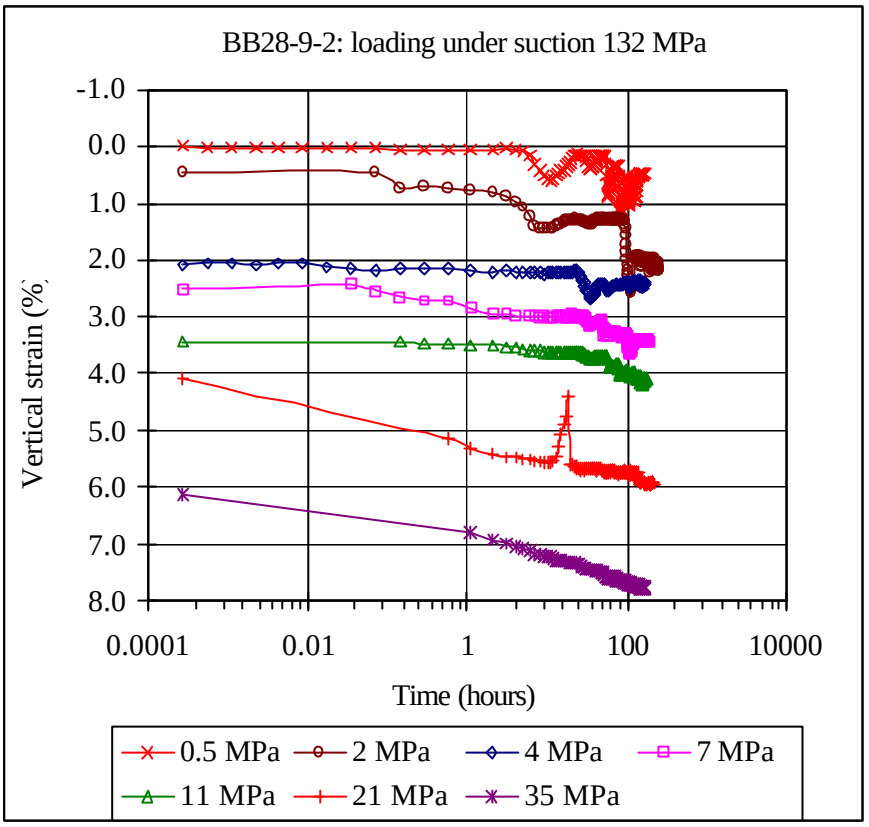

Figure 52: Evolution of strain during the different steps of the process of loading under suction 132 MPa for sample BB28-9A-2

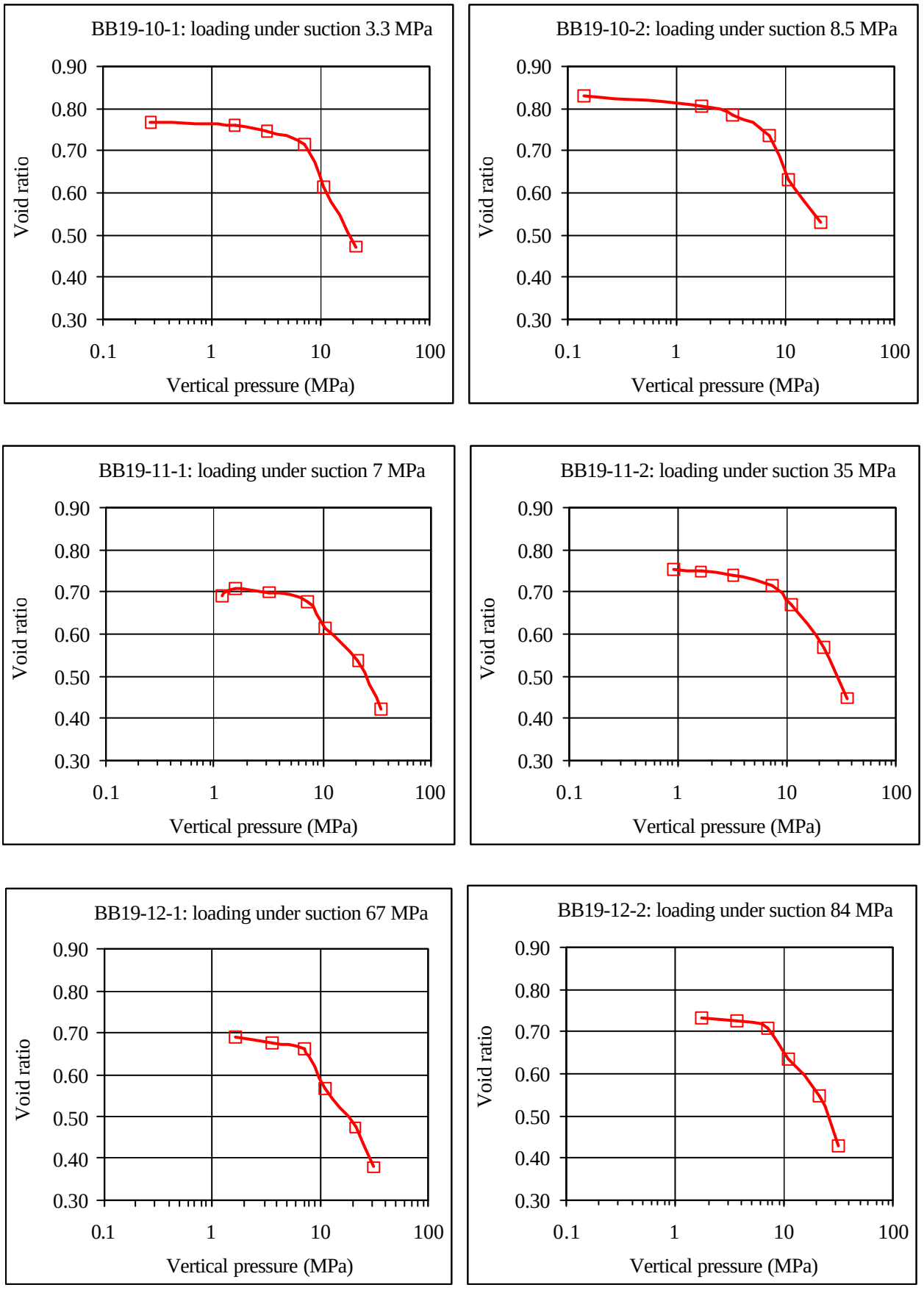

Figure 53: Oedometric curves of the tests performed in samples from section S19

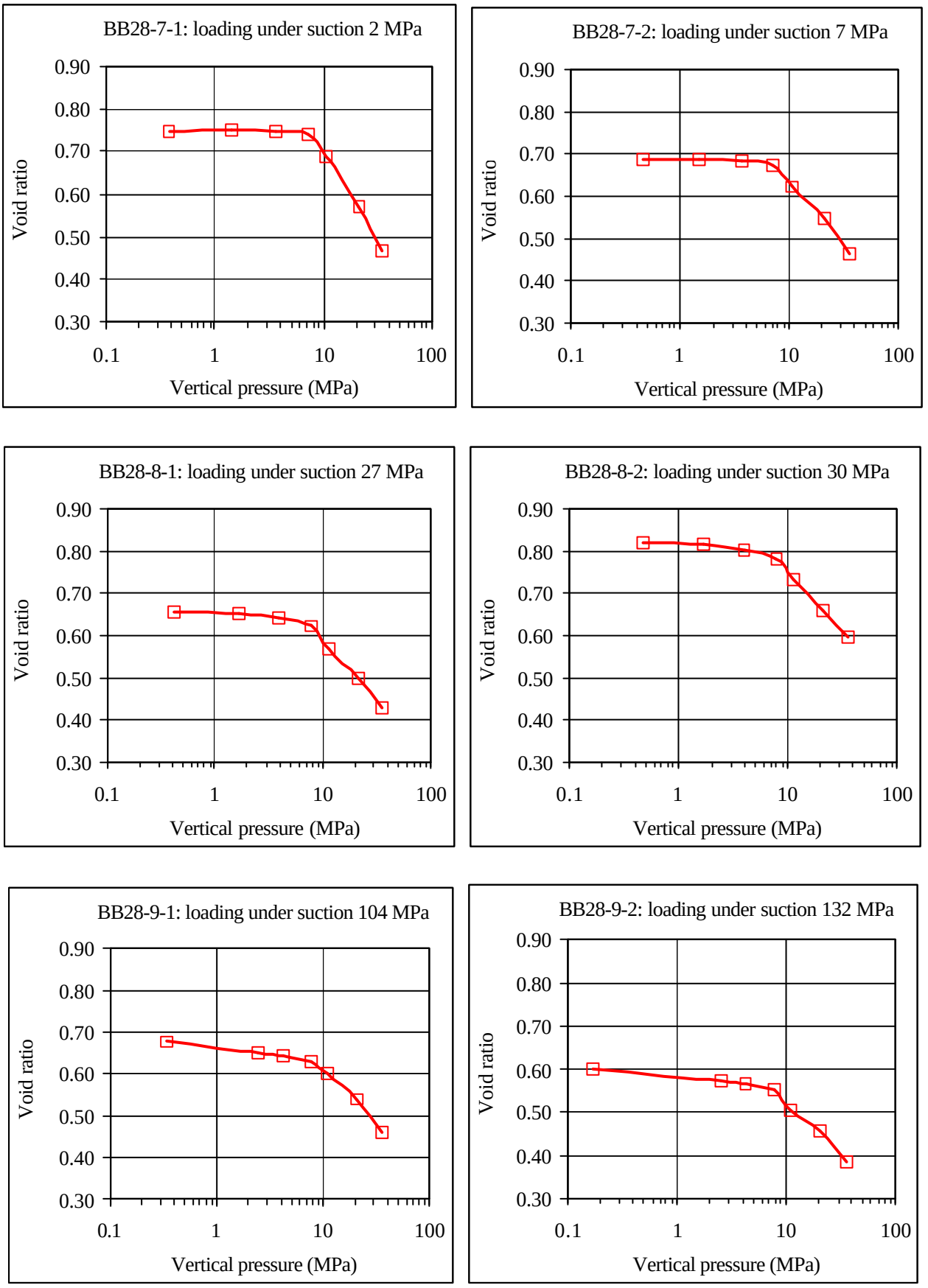

Figure 54: Oedometric curves of the tests performed in samples from section S28

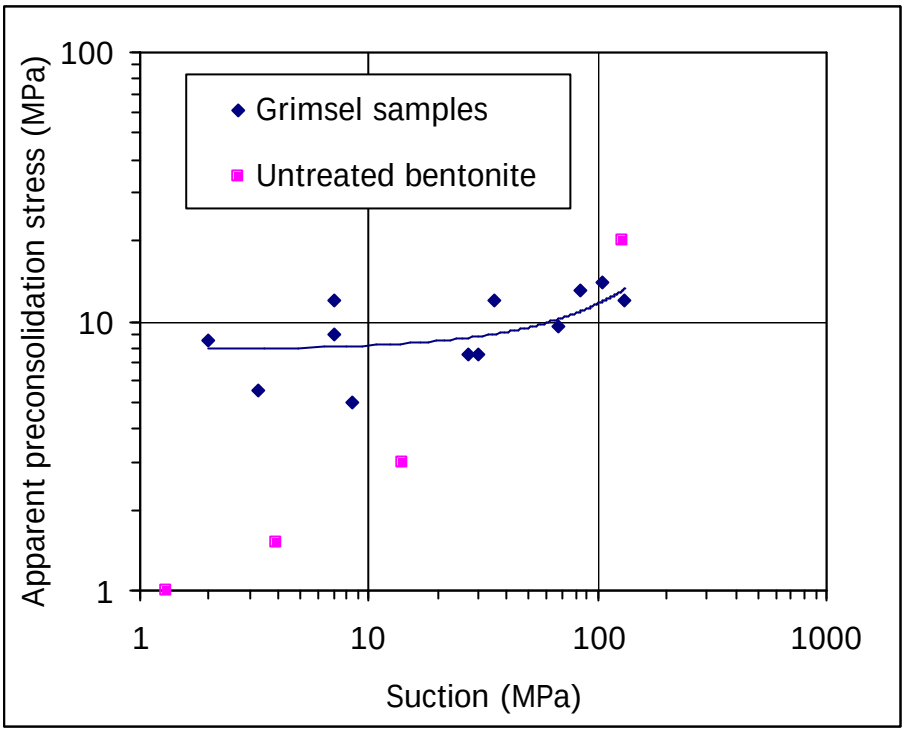

Figure 55: Apparent preconsolidation stress of samples from Grimsel and of untreated bentonite determined under constant suction corresponding to the water content of the clay

3.6. TESTS TO DETERMINE CHANGES IN THE THERMAL PROPERTIES

The superficial thermal conductivity has been measured in the sampled blocks before any other determination. The thermal conductivity has been measured over the surface of the block that faced the gallery entrance in two positions transversal to the radius, in order to have six measurements evenly distributed along the sampling radii (Figure 56). The results obtained are plotted in Figure 57, in which it can be seen that the values range within the interval 0.8-1.3 W/m·K. Higher thermal conductivities have been measured in the external blocks of the barrier, due to their higher water content.

Figure 56: Measurement of superficial thermal conductivity (the plastic foil is removed under the conductivity probe)

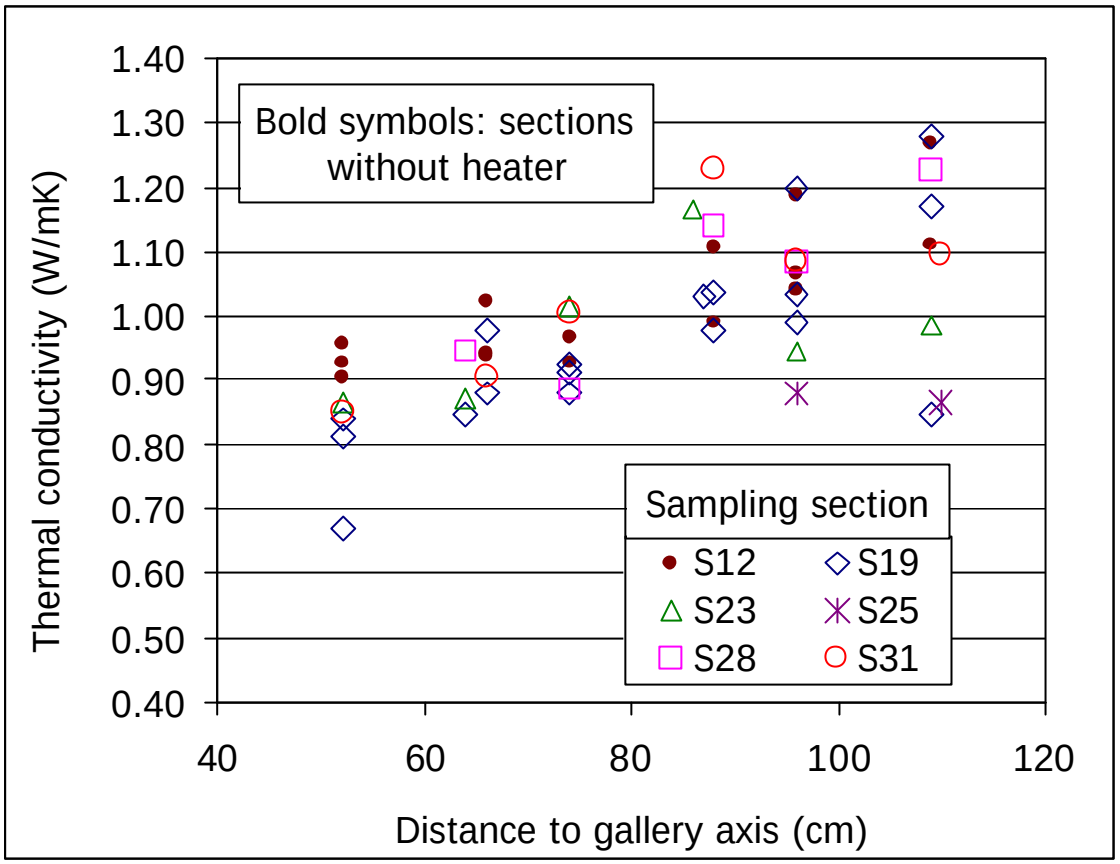

Figure 57: Thermal conductivity along radius of different sections

During FEBEX I measurements were performed on small blocks of bentonite compacted at different densities and water contents, with a view to checking the repercussion of both properties on the value of thermal conductivity (ENRESA 2000, Villar 2002). The granulated clay was used for compacting, either at hygroscopic water content or with added water. From the results obtained it was found that thermal conductivity (λ, W/m·K) may be related exponentially to water content (w, %) in the interval studied. This empirical relation, which also includes the contribution made by dry density (ρ_d, g/cm^3), is expressed as follows:

$$\ln \lambda = \ln (0.8826\ \rho_d - 0.8909) + 0.003\ w \qquad [6]$$

The theoretical thermal conductivity of the blocks from Grimsel has been calculated with this equation taking into account their dry density and water content. The values thus calculated have been compared to those actually measured. It has been observed that, in general, the "theoretical" values calculated with Equation 6 are a 6 percent higher than those measured. Figure 58 shows the values measured in blocks from Grimsel belonging to sections with heater as a function of their water content. The dry density of some of the blocks is indicated. Three lines obtained with Equation 6 corresponding to the theoretical thermal conductivity for three different dry densities are also drawn in the figure. It can be seen that the conductivities measured are in most cases below the expected values for blocks of the same dry density and water content. This can be clearly seen in Figure 59, in which the values actually measured and the theoretical values obtained with Equation 5 are directly compared. However, this is not the case for section S12, in which the heater was not present. On the contrary, the thermal conductivity values are slightly above those expected (Figure 60). In fact, if the deviations with respect to the theoretical value are calculated for the different

rings of the barrier (external, intermediate, internal) it is observed that the higher deviations are obtained in the blocks of the internal and intermediate rings, which present clearly lower conductivities than expected (Table XXII). To a lesser extent this is also observed in section S12. All these observations suggest that the decrease in thermal conductivity could be related to heating.

Table XXII: Deviation of the thermal conductivity values measured with respect to the theoretical values obtained with Equation 6

Position	Deviation (%)
Section S12 (no heater)	2
External ring of sections with heater	-5
Intermediate ring of sections with heater	-8
Internal ring of sections with heater	-10

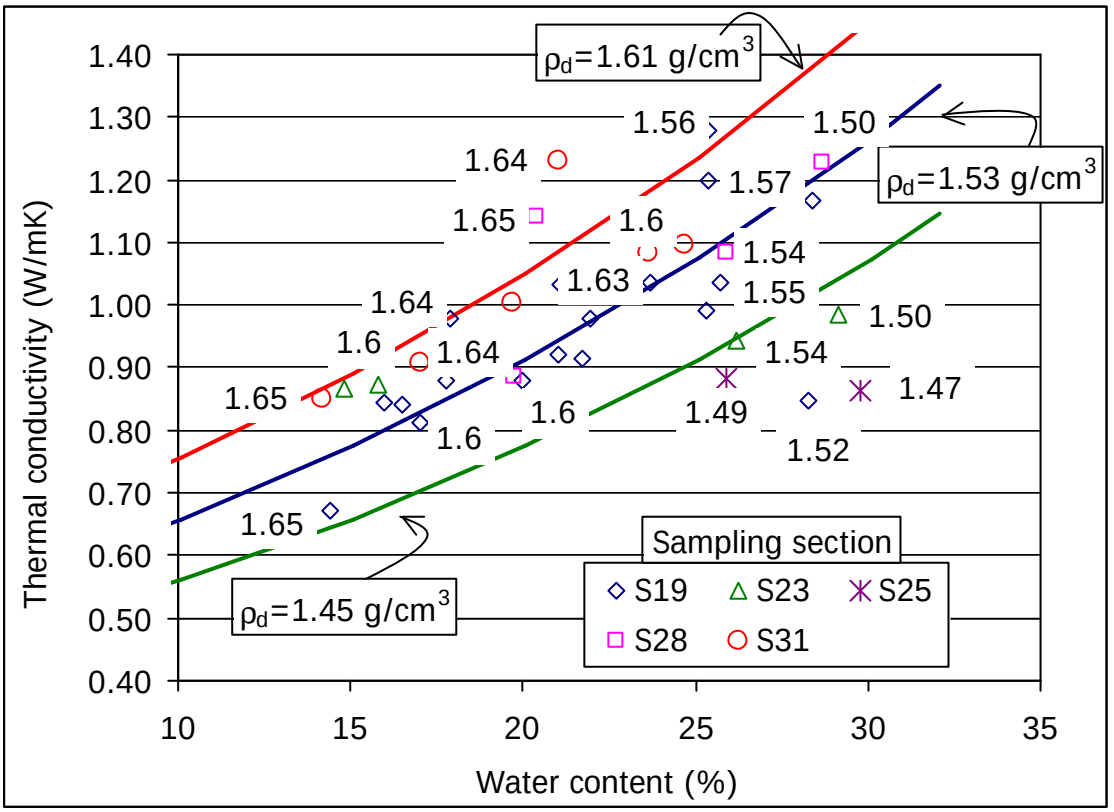

Figure 58: Thermal conductivity values measured in blocks from Grimsel (dry density indicated in g/cm^3) and theoretical fittings obtained with Equation 6

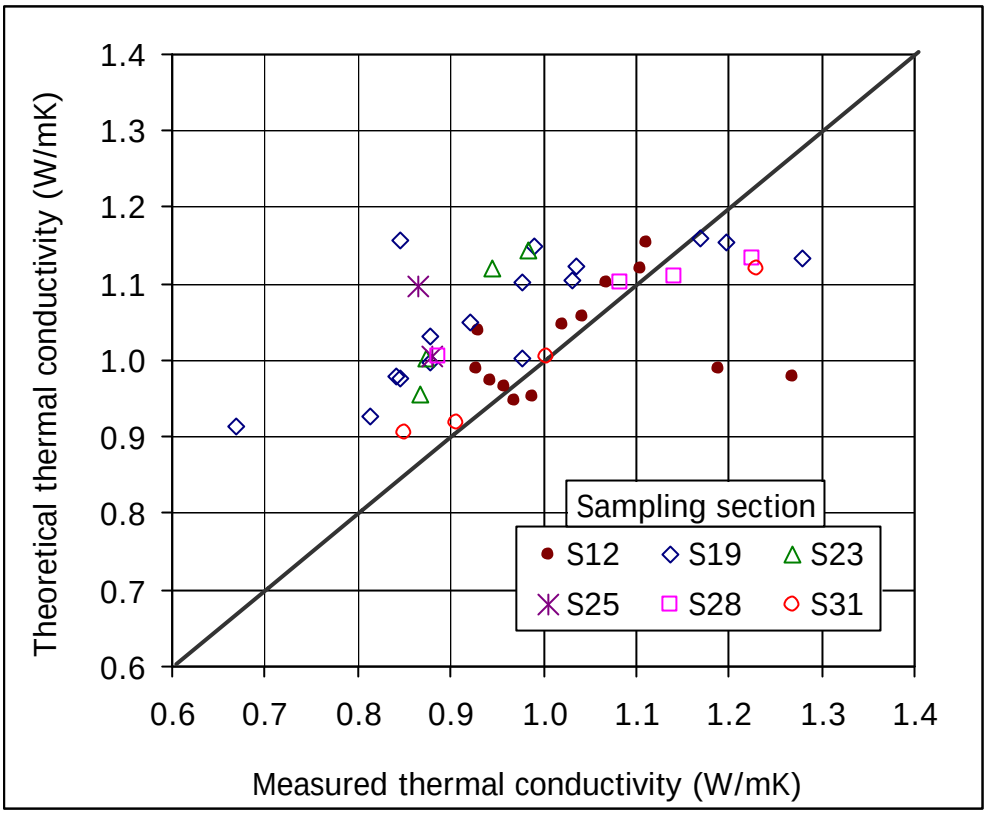

Figure 59: Thermal conductivity values measured compared to the theoretical values obtained with Equation 6

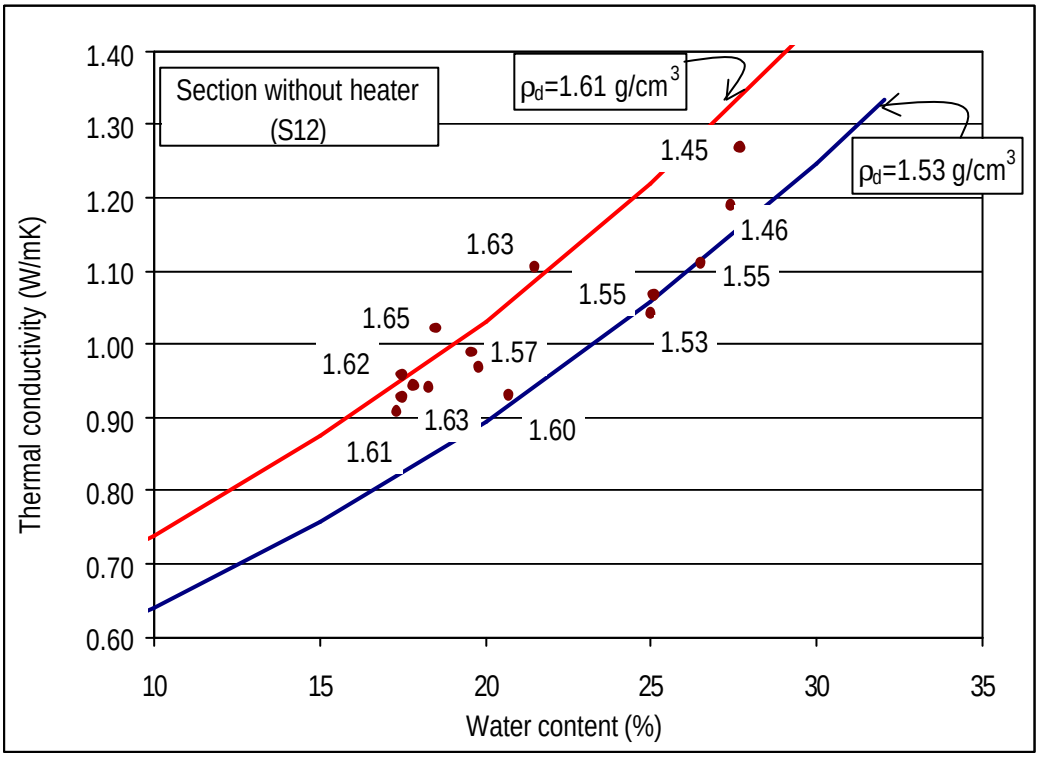

Figure 60: Thermal conductivity values measured in blocks from section S12 (dry density indicated in g/cm^3) and theoretical fittings obtained with Equation 6

4. SUMMARY AND CONCLUSIONS

After five years of operation, heater 1 of the FEBEX experiment at the Grimsel Test Site (GTS) was switched off in February 2002. Following cooling of the system during four months, the bentonite barrier was dismantled and the heater extracted. During dismantling many bentonite samples –in the form of cores or of complete blocks– were taken. Several determinations have been carried out in these samples with the aim of: (1) characterise the actual state of the bentonite and (2) determine the possible changes in its thermo-hydro-mechanical (THM) properties occurred during the experiment, due to the combined effect of temperature, water, joints and solutes. The results of the physical and THM characterisation performed at CIEMAT laboratories have been reported.

It must be taken into account that the state of the barrier has been analysed after four months of cooling, during which temperature and relative humidity were modified with respect to the values previous to the switching off (Figure 3 to Figure 5). To evaluate the actual physical state of the barrier after dismantling, the water content and dry density of numerous samples were determined, as well as their suctions. Besides the pore size distribution of some samples has been determined by mercury intrusion porosimetry. The following conclusions can be drawn:

- The distribution of water content and dry density in vertical sections presents an axial symmetry. The average values of water content and dry density in different vertical sections along the studied zone are similar. There are no major variations in overall water content between the sections around the heater and those out of it. The average degree of saturation for all the retrieved bentonite computed at CIEMAT laboratories is about 83 percent.

- There is a good agreement between the results obtained at the GTS immediately after retrieval of the blocks (Daucausse & Lloret 2003) and the results obtained at CIEMAT laboratories several months afterwards. This proves that the packing and transport procedures of the blocks have been the appropriate to keep their conditions even several months after retrieval.

- After being subjected for five years to repository conditions, the samples at the barrier have experienced an overall increase of volume, which implies a decrease of dry density from that of the compacted blocks, 1.70 g/cm^3, to an average density of the barrier of 1.58 g/cm^3. This is explained by the filling of all the construction gaps. However, the average value of dry density found is slightly lower than that given by AITEMIN upon construction of the barrier, 1.60 g/cm^3 (ENRESA 2000, p. 210). This could be a consequence of the slight decompression suffered by the barrier on dismantling and sampling.

- The overall drop in dry density is linked to a redistribution of pore sizes and an increase of the average pore size, which are not related to the position of the samples in the barrier. There has been a particular increase of the percentage of large pores (> 6 µm diameter) and a relative decrease of the percentage of smaller pores. However, the higher percentage of porosity –as in the case of the untreated blocks– corresponds to the size of less than 0.006 µm.

- The agreement between the gravimetric water contents measured (by oven drying) and the measurements of relative humidity recorded by the instrumentation installed in the bentonite blocks at Grimsel is good. On the other hand, the relative humidity of the blocks extracted has been measured in the laboratory with capacitive sensors. The comparison of the suctions thus measured agrees well with those recorded by sensors in Grimsel immediately before dismantling, what corroborates the inertia of the blocks to change their overall water content if they are well packed and the correct performance of the *in situ* sensors.

To fulfil the second objective, several thermal, hydraulic and mechanical properties of the retrieved bentonite were determined at the laboratory at room temperature. To evaluate the variation of hydro-mechanical properties of the bentonite after five years of TH treatment, the values obtained have been compared to those for the untreated FEBEX bentonite. Since the samples from Grimsel had different densities and water contents, it was necessary to have a complete database on the influence of these factors on the properties tested. The results obtained can be summarised as follows:

- The water retention capacity observed in the samples from Grimsel is similar to that of samples of untreated FEBEX clay compacted to the same dry density and subjected to similar suctions. This has been confirmed by measuring the suction of the blocks from Grimsel, what suggest that the retention capacity of the FEBEX clay has not appreciably changed after five years of being submitted to repository conditions.

- The hydraulic conductivity of the samples from Grimsel is clearly related to dry density and the latter in turn is related to the position of the block in the barrier. The values of hydraulic conductivity measured for the samples of lower density (more hydrated) are in the order of the theoretical ones, but for samples of higher densities there is a large dispersion in the values obtained without any clear tendency. This is probably due to the complexity of the experimental techniques applied, which increases for the higher densities, giving place to less accurate values.

- The final swelling strains upon saturation under a low vertical load of the samples coming from Grimsel are in the order of those expected for the untreated FEBEX bentonite compacted at the same initial dry density with the same water content. Consequently, it can be stated that the swelling capacity of the FEBEX bentonite has not changed irreversibly after five years of being subjected to repository conditions.

- Preconsolidation pressures lower than 10 MPa have been measured for all the Grimsel samples, being lower in the samples from the external ring of the barrier. It means an important decrease with respect to the initial preconsolidation pressure (around 40 MPa), the microstructural changes associated to the overall volume increase experienced during hydration accounting for that.

- Thermal conductivity has been measured in two different positions on the surface of around 30 blocks. Indeed, it increases with the water content of the clay and consequently it is higher for the blocks of the external ring. However, the blocks of the internal and intermediate rings present lower conductivities than expected according to the theoretical values. This suggests that there is a certain decrease in thermal conductivity related to heating.

5. ACKNOWLEDGEMENTS

Work co-funded by ENRESA and the European Commission, and performed as part of the Fifth EURATOM Framework Programme, key action Nuclear Fission (1998-2002), Project FEBEX II (EC Contract FIKW-CT-2000-00016). The laboratory work has been performed in the Soil Mechanics Laboratory of CIEMAT by R. Campos, J. Aroz and J.M. Durán.

6. REFERENCES

AITEMIN (2000) Test Plan FEBEX II Project. v1. FEBEX report 70-ST-H-0-4. Madrid.

AITEMIN (2002) Sampling plan for dismantling of section 1 of in situ test (Sampling Book). FEBEX Procedure 70-AIT-G-6-27 v.2. 114 pp. Madrid.

Bárcena, I, Fuentes-Cantillana, JL & García-Siñeriz, JL (2003) Dismantling of the heater 1 at the FEBEX in situ test. Description of operations. FEBEX report 70-AIT-L-6-03 v. 1. 123 pp. Madrid.

Daucausse, D & Lloret, A (2003) Results of "in situ" measurements of water content and dry density. FEBEX report 70-UPC-L-5-012. Barcelona.

CIEMAT (1999) Ensayos THM para el proyecto FEBEX. Internal report CIEMAT/DIAE/54111/9/99. FEBEX report 70-IMA-M-L-66. 115 pp. Madrid.

ENRESA (1995) Almacenamiento geológico profundo de residuos radiactivos de alta actividad (AGP). Diseños conceptuales genéricos. Publicación Técnica ENRESA 11/95. 105 pp. Madrid. (In Spanish).

ENRESA (1998a) Final design and installation of the in situ test at Grimsel. Publicación Técnica ENRESA 12/98. 184 pp. Madrid.

ENRESA (1998b) FEBEX. Bentonite: origin, properties and fabrication of blocks. Publicación Técnica ENRESA 4/98. 146 pp. Madrid.

ENRESA (2000) FEBEX Project. Full-scale engineered barriers experiment for a deep geological repository for high level radioactive waste in crystalline host rock. Final Report. Publicación Técnica ENRESA 1/2000. 354 pp. Madrid.

Fernández, AM & Rivas, P (2004) Task 141: Postmortem bentonite analyses. Geochemical behaviour. FEBEX report 70-IMA-L-0-109. 71 pp. Madrid.

Lloret, A, Villar, MV & Pintado, X (2002) Ensayos THM: Informe de síntesis. Internal report CIEMAT/DIAE/54111/9/99. FEBEX report 70-UPC-M-0-04. 97 pp. Barcelona.

Lloret, A, Villar, MV & Romero, E (in press) FEBEX Project. Final report on thermo-hydro-mechanical laboratory tests. Publicación Técnica ENRESA. Madrid.

Sing, KSW, Everett, DH, Haul, RAW, Moscou, L, Pierotti, RA, Rouquérol, J & Siemieniewska, T (1985) Reporting physisorption data for gas/solid systems with special reference to the determination of surface area and porosity. Pure & Appl. Chem. 57(4): 603-619. IUPAC.

Tuncer, ER (1988) Pore size distribution characteristics of tropical soils in relation to engineering properties. 2nd Inst. Conf. on Geomechanics in Tropical Soils 1: 63-70. Singapore.

UPC (1999) Ensayos THM para el proyecto FEBEX realizados por la UPC-DIT. Internal report UPC-FEBEX 70-UPC-M-0-03. 157 pp. Barcelona.

Villar, MV (2000) Caracterización termo-hidro-mecánica de una bentonita de Cabo de Gata. Ph. D. Thesis. Universidad Complutense de Madrid. 396 pp. Madrid. (In Spanish).

Villar, MV (2001) Ensayos termohidráulicos en celdas grandes: propiedades hidro-mecánicas. Internal report CIEMAT/DIAE/54520/1/00. FEBEX report 70-IMA-L-0-76. 65 pp. Madrid.

Villar, MV (2002) Thermo-hydro-mechanical characterisation of a bentonite from Cabo de Gata. A study applied to the use of bentonite as sealing material in high level radioactive waste repositories. Publicación Técnica ENRESA 01/2002. 258 pp. Madrid.

Villar MV, Fernández AM, Hernández AI, Muurinen A, Pacovský J, Montenegro L, Gourry JC, Lloret A, Verstricht J, Villieras F & Robinet JC (2002a): Work proposal for task 141: Postmortem bentonite analysis. FEBEX report 70-IMA-H-6-16 v1. 35 pp. Madrid.

Villar, MV, Martín, PL, Lloret, A & Romero, E (2002b) 2nd Report on Thermo-hydro-mechanical laboratory tests. Deliverable D-17/2. September 00-March 02. May 2002. CIEMAT/DIAE/54520/6/02. FEBEX Report 70-IMA-L-0-97. 53 pp. Madrid.